

University of Alberta

**Highly Ordered Methanofullerene Nanotube Array: Fabrication and
Implications for Room Temperature Organic Spintronics**

by

Ryan Starko-Bowes

A thesis submitted to the Faculty of Graduate Studies and Research
in partial fulfillment of the requirements for the degree of

Master of Science

in

Solid State Electronics

Electrical and Computer Engineering

© Ryan Starko-Bowes

Fall 2013

Edmonton, Alberta

Permission is hereby granted to the University of Alberta Libraries to reproduce single copies of this thesis and to lend or sell such copies for private, scholarly or scientific research purposes only. Where the thesis is converted to, or otherwise made available in digital form, the University of Alberta will advise potential users of the thesis of these terms.

The author reserves all other publication and other rights in association with the copyright in the thesis and, except as herein before provided, neither the thesis nor any substantial portion thereof may be printed or otherwise reproduced in any material form whatsoever without the author's prior written permission.

Abstract

Organic semiconductors have come to the forefront of research in physics, chemistry and electronics due to their impressive properties and low cost of device production. Presented here is a novel centrifuge assisted organic nanowire growth technique and its application in the fabrication of methanofullerene ([6,6]-phenyl-C₆₁-butyric acid methyl ester (PCBM) nanotube array spin valves. This growth technique enables the fabrication of a wide range of potential organic nanowire devices for applications in photonics, optoelectronics and spintronics. In particular, spin valves of PCBM nanotube arrays fabricated using this technique demonstrate encouraging spin transport properties. In spite of a long channel length (~325 nm), these devices exhibit an inverse spin valve effect which persists even at room temperature. The spin relaxation length in these devices is estimated to be ~50 nm at room temperature which is the largest room temperature spin relaxation length in organic nanowire systems reported to date, including carbon nanotubes.

Acknowledgment

Firstly I would like to thank my supervisor Dr. Sandipan Pramanik. He sparked my interest in research and is the reason I decided to pursue graduate studies. Thank you for all your guidance throughout the past 3 years and for giving me the freedom to explore so many interesting projects.

Thank you to my group members Srikrishna Bodepudi, Abhay Singh and Kazi Alam. All of you have given me guidance and dedicated time and effort to helping me in my own projects as well as course work. I would not have been able to complete these projects or make it through this degree without you. I am truly grateful for all you guys have done for me and wish you all the best in your studies as well.

To my friends, my graduate years have been full of great memories and I have all of you to thank for that. To my family, your continuous support and interest in my research make what I do very rewarding. You have done so many things for me that have allowed me to focus on my work and have encouraged me to follow my passions. And finally to my girlfriend Larisa, I cannot thank you enough for all that you have done for me. I am lucky to have such a genuinely thoughtful person in my life.

Table of Contents

Abstract.....	i
Acknowledgment	ii
List of Figures	v
Chapter 1. Introduction	1
1.1 Introduction to Organic Electronics.....	1
1.2 Organic Nanowires	2
1.3 Current Fabrication Methods of Organic Nanowires.....	3
1.3.1 Electrospinning	3
1.3.2 Nanolithography	4
1.3.3 Physical Vapour Deposition.....	6
1.3.4 Self-Assembly.....	7
1.3.5 Template Based Fabrications	8
1.4 Motivation of this Work.....	9
1.5 Work Completed to Date	12
1.5.1 Novel Centrifuge Assisted Template Wetting Method.....	12
1.5.2 Spin Valve Effect in PCBM Nanotube Arrays	13
1.6 Future and Ongoing Work	13
Chapter 2. Nanoporous AAO Template Fabrication, Organic Nanowire Growth and Device Production Process Flow	15
2.1 Summary	15
2.2 Background.....	15
2.3 Fabrication Protocol.....	19
2.4 Discussion on Centrifuge Assisted Template Nanowire Growth	29
2.4.1 Physical Picture for Nanowire Growth	29
2.4.2 Critical Parameters.....	30
2.4.3 Potential Benefits and Drawbacks	32
2.4.4 Future Directions, Modification and Potential Applications	33
Chapter 3. Magnetoresistance Study of PCBM Nanotube Spin Valves	34
3.1 Summary	34
3.2 Introduction.....	34
3.3 Device Fabrication.....	35

3.4 Device Characterization.....	38
3.4.1 Raman Characterization of PCBM Nanotubes	38
3.4.2 XRD Characterization of PCBM Nanotubes	39
3.5 Charge Transport Measurements	40
3.6 Magnetoresistance Measurements	44
3.7 Effect of Contacts on Magnetoresistance	52
3.8 Magnetoresistance of [Ni film – PCBM nanotube – Co nanowire] Samples Exhibiting Linear I-V Characteristics:.....	53
3.9 Conclusion	54
Chapter 4. Future/Ongoing Work	55
4.1 Improving Spin-Valve Response	55
4.2 Hybrid Metamaterials	57
4.3 Coaxial Organic Nanowires for Radially Heterojunctioned Photovoltaic Devices	58
References.....	60
Biography.....	68

List of Figures

Figure 2.1 Schematic description of the organic nanowire synthesis. Steps (a) – (e) represents multi-step anodization and etching for fabrication of well-ordered nanopores. Step (f) represents organic nanowire growth.	20
Figure 2.2 FESEM image of empty template anodized on Al foil. Main image shows pore structure while inset shows a cross section of the pores with barrier layer present at bottom.	22
Figure 2.3 Anodization current as a function of time. For the final step of anodization on glass substrate, current rises when the entire aluminum is consumed and the electrolyte comes in contact with the underlying Au layer.....	23
Figure 2.4 FESEM image of empty template anodized on Al thin film on glass. Main image shows pore structure while inset shows a cross section of the pores with layered structure (500 nm porous Al ₂ O ₃ / 7 nm Au / 20 nm TiO ₂ / glass substrate).	24
Figure 2.5 Schematic of the centrifuge and loading of the empty template in the test tube for organic nanowire growth.....	26
Figure 2.6 FESEM of PCBM nanotubes. Main image shows a cross section of the template with the entire length of the pore filled with PCBM, displaying the hollow nature of the tubes. Inset is a normal view of the bottom side of the template after the barrier layer has been removed. This shows a capped end to the nanotube.....	27
Figure 2.7 FESEM of metallic nanowires grown inside AAO template. Main image is of a field of Ag nanowires grown in AAO template on glass after the matrix has been removed. Inset is a cross section of Co nanowires grown in the pores of AAO on foil substrate with PCBM nanotubes grown on top.....	28
Figure 3.1 Schematic of final PCBM nanotube spin valve array device structure.	36
Figure 3.2 FESEM of the PCBM nanotube tips at the interface with bottom Co nanowires. It is evident the PCBM nanotubes are closed at the bottom.	37
Figure 3.3 FESEM of cross section of final tri-layer (Co nanowire/PCBM nanotube/Ni thin film) device.....	38
Figure 3.4 Raman spectrum of PCBM nanotubes imbedded in Al ₂ O ₃ template.	39
Figure 3.5 XRD spectrum of PCBM powder and PCBM nanotubes imbedded in the AAO matrix.	40

Figure 3.6 (a)-(c) Typical temperature-dependent current (I) vs. voltage (V) characteristics of ~ 325 nm long PCBM nanotubes embedded in alumina matrix. (d) Conductance (dI/dV) vs. voltage (V) characteristics for the devices in (b)..... 41

Figure 3.7 (a) Temperature dependence of ideality factor of diodes in spin-valve structure. (b) Rigid energy band diagram for the spin valve device and schematic description of the charge transport process..... 43

Figure 3.8 Magnetoresistance scans of [Co nanowire/PCBM nanotube/Ni] spin valves (without interfacial alumina barrier) for (a) 25K, (b) 175K, (c) 200K, and (d) 290K. MR is defined as $(R(B)-R_{max})/R_{max}$. The PCBM nanotube length is ~325 nm and magnetic field is parallel to the direction of current. The arrows indicate the (inverse) spin valve peaks. 45

Figure 3.9 Magnetoresistance measurements of [Co nanowire/PCBM nanotube/alumina barrier/Ni] spin valves for (a) 30K, (b) 80K, (c) 150K, and (d) 250K. As before, the PCBM nanotubes are ~325 nm long, magnetic field is parallel to the direction of current, and MR is defined as $(R(B)-R_{max})/R_{max}$. The arrows indicate the (inverse) spin valve peaks. 47

Figure 3.10 Magnetoresistance traces for the spin valve samples with longer average PCBM tube length of ~332 nm. As expected, the spin valve peaks are weaker than the previous cases (at similar temperatures) where the PCBM tube length was shorter (~325 nm). The arrows indicate the locations of the spin valve peaks..... 48

Figure 3.11 Spin relaxation length as a function of temperature for two sets of samples. Average length of PCBM nanotubes is ~ 325 nm in one set and ~ 332 nm in the other set. The error bars represent the variation in estimated spin relaxation length due to ~10% variation in the PCBM nanotube length..... 50

Figure 3.12 Effect of contacts on magnetoresistance. (a) Anisotropic magnetoresistance traces for the [Co nanowire/Ni] bilayered control samples, which have no PCBM layer. Typical positive magnetoresistance effect is observed, which occurs when magnetic field is parallel to the direction of current. (b), (c) Magnetoresistance measurements on trilayered samples with only one ferromagnetic contact. No spin-valve peaks have been observed, but the negative background magnetoresistance is present. (d) Magnetoresistance measurements on trilayered samples with no ferromagnetic contact. The background magnetoresistance is still present in this sample..... 53

Figure 3.13 Absence of spin valve effect in Ni-PCBM-Co devices that exhibit linear I-V response. 54

Figure 4.1 Schematic of proposed structure of metal-organic hybrid nanowire metamaterial device. 58

Chapter 1. Introduction¹

1.1 Introduction to Organic Electronics

Semiconducting materials have been the key to the creation of our electronics and computer industry. Inorganic semiconductors such as germanium, silicon and gallium arsenide were the first used in electronic devices. Silicon has so far dominated the mainstream electronics market and is used in almost every device from computers and smart phones to solar cells and even digital watches. Traditionally, organic polymers and small molecules have been considered insulators as they have difficulty conducting current. This school of thought has changed drastically within the last 30 years as organic semiconductors have become a hot topic for research. The spark that ignited such interest in the field can be credited to the Nobel prize winning work of Heeger, MacDiarmid and Shirakawa [2]. They found that by doping polyacetylene with arsenic pentafluoride (AsF_5), they could change the conductivity of the material by a factor of 10^{11} , effectively creating the field “plastic electronics” [2].

Generally, organic matter is comprised of a combination of carbon and hydrogen atoms but typically includes other common elements such as nitrogen, oxygen, phosphorous, sulfur or others. The first organic materials discovered to have conductive properties were π -conjugated organic polymers [2]. Charge transport in these materials is enabled by the delocalization of the π -bonds in the carbon backbone of the polymer chain [3]. Organic electronics has come a long way since then with an ever expanding library of materials that now includes oligomers and small molecules such as tris(8-hydroxyquinolino)aluminum (Alq_3), rubrene (5,6,11,12-tetraphenylnaphthacene) and fullerene (C_{60}). In addition to resonance stability, phonon assisted hopping can be a dominant mechanism for charge transport in these materials [4].

Recent advances in the field of organic semiconductors have been fuelled by potential low cost manufacturing and the ability to design and tailor organic

¹ Portions of this chapter have been published in ref [1]

materials' molecular structure to the needs of the device or application [5], [6]. The molecular structure can now be engineered to tune fundamental material properties such as HOMO/LUMO levels, band gaps, Fermi levels, optical absorption spectra, exciton diffusion length, spin diffusion length etc. [6].

1.2 Organic Nanowires

The interdisciplinary field of nanotechnology has exploded in the last two decades due to the remarkable effects exhibited by materials when their physical dimensions are confined to the nanometer scale [5]–[7]. This has enabled us to create 2D, 1D and 0D nanostructures that exhibit significantly different performance characteristics than their bulk counterparts. This is typically a result of achieving specific structures, high surface to volume ratios and sometimes quantum confinement. To date, the majority of attention in this field has focused on the fabrication of such nanostructures using inorganic semiconductors, which has given us exceptional control over material properties and device performance. For example quantum dots created out of the same material can fluoresce in a wide range of colours depending on the specific nanoscale size of the dots [8].

Nanowires composed of organic semiconductors are recently attracting increasing interest since this geometry often offers enhanced device performance. For example, in case of organic solar cells, a promising method of improving efficiency is to achieve nanometer scale interpenetrating networks of donor and acceptor materials, with an interfacial distance smaller than the exciton diffusion length (~10–20 nm) in the organic. An ideal configuration that has been proposed for these cells consists of an array of vertically aligned donor organic nanowires attached to an electrode and surrounded by an acceptor type organic connected to another electrode [9]–[14]. Similarly, electrical properties of organic nanowires can be tuned by varying the nanowire geometry [15] and can potentially be exploited to develop high-performance transistors that rival the performance of amorphous silicon [16]. Finally, another area where organic nanowires have recently emerged as a promising candidate is the relatively new field of “organic spintronics” [17]–[19]. Organic materials, due to their weak spin-orbit and

hyperfine interactions offer an attractive platform in which spin memory of a carrier can be preserved for sufficiently long time [20], [21]. This makes organics a suitable host for spin-based classical and quantum bits [20], [21]. The chemical composition of the organics and molecular packing can be changed to control the strengths of these interactions [22], [23] and hence spin lifetime is tunable in such systems. Further, nanowire geometry allows identification of the dominant spin relaxation mode in organics [20] and investigation of spin-phonon coupling [24], the knowledge of which is a crucial ingredient for room-temperature organic spintronics [25].

1.3 Current Fabrication Methods of Organic Nanowires

In this work we have developed a template-assisted method to fabricate organic nanowire arrays. However, there are several other methods available to fabricate different sizes of organic nanowires of different material such as electrospinning, nanolithography, physical vapour deposition (PVD) and self-assembly, which will be discussed here. These techniques all have their advantages and disadvantages and may be able to serve a niche application. However, advantages of our template based technique, such as low cost, ease of fabrication, high degree of nanowire alignment, high throughput and the ability to fabricate axially and radially heterostructured organic and metal-organic hybrid nanowires suggest it is a better candidate for use in a number of applications.

1.3.1 Electrospinning

In electrospinning, a syringe with a very fine capillary outlet is held ~5-50 cm from a grounded collecting plate. The syringe, and hence the solution inside the syringe, is held at a high voltage such that the electric field is of the order 10^5 V/m. The charged solution in the syringe will be attracted to the grounded plate and the capillary will eject a steady stream of solution once the capillary force and surface tension is overcome by the electrostatic force imposed on the system. The shape and orientation of the produced nanowire is determined by the motion of the grounded collector, which can be designed to produce many different structures. The process will form continuous nanowires on the collector if the

solution is viscous enough. The diameter of the fiber produced shrinks from ~ 100 μm at the capillary outlet to $\sim 10\text{nm}$ - $10\mu\text{m}$ on the collector once the solvent has evaporated with potential lengths ranging from centimeter to kilometers, resulting in extremely high aspect ratios [6], [26], [27].

Traditional electrospinning uses a DC bias to propel the jet of material towards the collecting plate. However, this introduces fiber instability or “whipping” caused by repulsive forces within the charged material [6], [27], [28]. Depositing nanowires on insulating substrates also becomes a challenge when using a DC bias. To resolve these shortcomings, an AC bias can be used. This has demonstrated reduced fiber whipping, improved fiber alignment and deposition on insulating substrates [28].

Functional electronic devices such as FETs, rectifying diodes, electroluminescent devices and electro chromic devices have been explored using electrospun organic nanofibers. However, as only one nanofiber can be produced per capillary outlet, throughput of this method is not ideal for large scale production [6].

1.3.2 Nanolithography

Nanolithography is a process very common in inorganic semiconductor processing and is used today to produce the majority of our electronic device. In general it uses a master pattern to create multiple copies of the same design. Several different forms of nanolithography exist and have been used to fabricate organic nanowires such as electron beam lithography (EBL), scanning probe lithography (SPL), imprint lithography and others.

In photolithography, UV light is exposed to a thin polymer film such as poly(methyl methacrylate) (PMMA) to modify the chemistry of the polymer material making a pattern in the layer that shows after subsequent development in a suitable solution. The feature size of photolithography is limited by the diffraction limit of UV light. EBL uses electrons to pattern the polymer layer or resist, which have a smaller wavelength than UV light and are able to produce smaller features. EBL can be used to fabricate organic nanowires in two ways.

The first is called lift-off, where a sacrificial layer of resist is exposed and developed to create the desired pattern. Organic material is then deposited on top of the resist using spin coating or by immersing the substrate in a solution of the material. The organic will cover the layer of resist as well as fill the voids where it has been developed (removed). Removal of the remaining resist leaves only a pattern of organic material that has been defined by the electron beam. Nanowires with widths from ~80-150 nm have been produced using lift-off EBL [6], [29], [30]. The second method of using EBL to produce organic nanowires is to expose the electron beam directly to a thin film of the semiconducting polymer. The electron beam increases cross linking between molecules in the organic thin film (as well as in resists), which decreases solubility in solvents allowing the 1D structures to remain on the substrate while the rest of the thin film is dissolved. Additional agents can be added to the organic solution to increase cross linking when exposed to electron beams, enhancing the insolubility of exposed material. Direct EBL has been able to produce line widths of ~50-70 nm [6], [31]. In both processes only one beam of electrons with very fine width is used and must raster back and forth across the surface to transfer the desired pattern. Because of this, EBL is a very time consuming and low throughput technique.

Scanning probe lithography (SPL) is another form of nanolithography that can be applied to accommodate organic materials and produce semiconducting organic nanowires. Again, there are two different types of SPL, dip-pen lithography and chemical patterning. Dip-pen lithography is very analogous to writing with a pen, where an atomic force microscope (AFM) tip is used as the pen and an organic polymer solution is the ink. As the name implies, the AFM tip is dipped in to the solution and the solution adsorbs to it. The tip is then transferred to the substrate where it writes the solution on to the substrate. As the tip can only adsorb so much solution, the amount of solution on the tip is a limiting factor in the length of any produced nanowire. The second method is to use the AFM tip to pattern a thin film of organic material that has already been deposited. This is typically done electrochemically by applying a voltage to the conductive AFM tip and keeping the sample grounded or thermo-chemically by local heating of the

organic thin film induced by a hot AFM tip or metallic nanowire. This causes cross linking of the organic materials' molecules or polymer chains which will define the nanowires for later processing. Widths of ~28 nm and ~45 nm were achieved for thermochemical and electrochemical methods respectively [6], [32], [33]. Again, SPL is a low throughput technique as the AFM tip needs to scan across the substrate and “draw” the pattern to be transferred, which is very time consuming.

The last nanolithography technique that will be presented here is nanoimprinting lithography (NIL), also known as embossing. NIL uses a rigid master mold to transfer a pattern in to a deposited material or thin film. Organic nanostructures can be fabricated using this method by pressing a mold in to a thin film of organic material at high temperature and pressure. Typical nanowires with line widths of ~ 10-100 nm have been fabricated using this method [6], [34], [35]. The greatest strength of NIL is its ability for high throughput and low cost of production. Because there is only one step to press the mold in the film to be patterned, there is no writing or rastering involved as in previously described methods, allowing NIL to pattern many devices on a large area substrate simultaneously.

1.3.3 Physical Vapour Deposition

Although they are in some sense similar, two physical vapour deposition (PVD) techniques exist that have been modified to accommodate the deposition of organic materials, which are evaporation and chemical vapour deposition (CVD).

In evaporation, a vacuum chamber containing the substrate and a crucible with the organic source material to be deposited is pumped down to a high vacuum ($\sim 10^{-7}$ Torr). Once the chamber reaches the desired pressure, it is sealed off and the crucible is heated by an element or electron beam so that the source material reaches vapour phase temperatures at the relative pressure. Once in vapour phase, a flux of source material travels by diffusion from the crucible to the substrate where it deposits a thin film.

CVD is similar to evaporation in that a crucible of source material to be deposited is heated to create a vapour. In CVD, this usually takes place in a quartz tube with a geometry such that the substrate is located some distance down the tube from the crucible. Near the crucible, a stream of inert gas (Ar, N etc.) is injected in to the tube at low pressure through an inlet. The gas flows through the tube, facilitating the transport of source material from the heated region in the quartz tube to the substrate, located in a cooler region down tube from the source. As the source material reaches the substrate, it condenses on the relatively cool substrate for deposition [6].

Both of these deposition methods will create films that conform to the morphology of the substrate. Typically, when done on a flat substrate, this will result in a thin film of organic material. Continuous organic thin films of materials such as Alq₃ can be deposited with thicknesses as thin as 1-2 nm [36]. Although thinner organic films have been reported (~0.06 nm) [37], they are likely not continuous because the percolation threshold of various material-substrate combinations makes it very difficult to avoid the formation of islands and obtain a continuous film. This can later be patterned using one of the techniques in section 1.3.2., or others, to achieve organic nanowires. Alternatively, a substrate can be pre-patterned in to a template for the material to fill, creating nanowires. Depending on the device function, the template can then be left or removed to disperse nanowires in solution. The problem with PVD when trying to fill a template with material is that a vapour can only penetrate so far in to a feature before it will deposit on to the wall, making the fabrication of high aspect ratio structures, such as nanowires, extremely difficult.

1.3.4 Self-Assembly

Self-assembly is potentially the most powerful method of fabricating organic nanowires and nanostructures. Organic molecules and polymers in solution can spontaneously align themselves to form a variety of nanostructures including nanowires depending on the nature of the environment [38], [39]. We can use the difference in solubility of a specific molecule to promote self-assembly of

nanostructures when transferred from one solvent to another, or by varying the temperature of the solvent. As the environment the molecules are surrounded by changes, the molecules can begin to bond with each other, forming nanostructures. There are several types of intermolecular bonding that can facilitate self-assembly such as π - π stacking, dipole-dipole interaction, van der Waals forces, hydrogen bonding and hydrophobic interactions [6]. Some of these forces are anisotropic in nature which will lead to the formation of 1D nanostructures or nanowires. As the molecules begin to crystallize when transferred to a new solution or upon cooling, they will precipitate out of the solution and can then be extracted [40]–[42]. Because of the bottom-up nature of this fabrication method, extremely well ordered molecular structures and large crystal sizes are possible which will result in outstanding electronic properties.

For example, hexathiapentacene (HTP) in a solution of hot benzonitrile will spontaneously form nanowires of length $\sim 50 \mu\text{m}$, height $\sim 470 \text{ nm}$ and width $\sim 1 \mu\text{m}$ when cooled to room temperature [6], [43]. Triisopropylsilylethynyl pentacene (TIPS-PEN) nanoribbons for organic transistors were also fabricated using the solvent exchange method producing ribbons of height 100-600 nm, width 4-13 μm and length 40-800 μm [6], [42]. While this method can produce structures with unmatched electrical performance, it is difficult to incorporate this with other fabrication techniques to produce functional devices, which is this fabrication technique's biggest challenge.

1.3.5 Template Based Fabrications

Template based fabrications in general use a mould or template around which organic nanostructures can be formed. While there are several different types of templates that can be used [44], [45], I will focus on nanoporous templates as that is what this thesis is based on. There are two main types of nanoporous templates, Particle Track-Etched Membranes (PTM) [46], [47] and Anodic Aluminum Oxide (AAO) membranes [1], [48].

PTMs use a combination of irradiation or bombardment from charged particles on thin film substrates and later chemical etching to form nanopores. Ions penetrate

the full thickness of the film leaving tracks with latent ions [49]. The etching only affects the areas where ion bombardment has occurred, leaving the bulk of the film unaffected. Pores of diameter $\sim 15\text{ nm} - 1\ \mu\text{m}$ [6], [46], [50] can be fabricated with specific placing of pores. PTMs have their place in nanofabrication but lack channel uniformity, location control, pore density and have poorly ordered pore structure which makes them a weak candidate for many applications [48].

AAO templates are created by electro chemically oxidizing (anodizing) a thin film or foil of aluminum. As the surface of the film or foil is oxidized, nanopores are spontaneously formed in the oxide film (Al_2O_3), which self-assemble themselves in a 2D honeycomb lattice. By varying anodization conditions such as bias, electrolyte solution or run time we can control structural parameters of the final nanoporous template such as pore diameter, interpore spacing and template thickness. Pore sizes ranging from $5\text{ nm} - 270\text{ nm}$ [1], [6], [48] can be fabricated using this technique and the nanopores spontaneously pack themselves to achieve a high density.

To fabricate organic nanowires using either of these two templates, we need to fill the fabricated cylindrical pores with the desired organic materials. Because most organic powders can be dissolved in some form of solvent, this is typically the vehicle used to transport organic material in to the pores. Templates are either dipped in the organic solution and dried or drops of the solution are placed on the template surface while capillary forces pull the solution in to the pores. For more details on this fabrication technique, refer to Chapter 2 which presents in depth organic nanowire fabrication using AAO templates.

1.4 Motivation of this Work

There are many potential applications that could make use of organic nanowires such as organic FETs, organic spin valves, plasmonics or organic photovoltaic devices. This thesis focuses on organic spin valves and plasmonics. An array of these vertically aligned organic nanowires is used as the active layer of an organic spin valve device for potential application in organic magnetic random access memory (O-MRAM). This organic nanowire array can also be fabricated on glass

substrates such that the material can interact with light for photovoltaic and plasmonic devices. This thesis explores a novel organic nanowire fabrication method and its application in spin valves and plasmonics.

In most previous studies on organic spintronics, mainly vacuum deposited or spin-coated organic *thin films* have been employed. However, for second generation low-cost, printable and rollable “molecular spintronic” memories, *high-density integration* of organic spin valves and their *room temperature operation* is required. In spite of significant advances at a single device level, high-density integration of organic spin valves is largely underdeveloped. We note that despite large room temperature tunneling magnetoresistance in organic-based magnetic tunnel junctions, they are not particularly suitable for very large scale integration. This is mainly due to the facts that device resistance is inversely proportional to the junction cross-section and the design requirement of low device resistance necessitates fabrication of thinner tunnel junctions [51]. Thickness control is challenging when the barrier is thin and especially when the barrier consists of organic layers. Such thin organic films are prone to pinhole shorts due to non-uniform surface coverage [52], and more importantly as a result of deposition of the top ferromagnetic contact, when significant amount of ferromagnetic clusters interdiffuse within the soft organic [17], [18]. Thicker devices also allow additional tailoring of the carrier spin orientations during transport, thus opening the possibility of three-terminal organic devices. Thus alternative device geometries and material systems need to be explored which will allow scalability as well as room temperature operation.

In this work we consider *vertically oriented nanotube geometry* [53], [54] for fabrication of organic spin valves since individual devices have nanoscale footprint and they can, in principle, lead to unprecedented bit densities approaching Tb/cm². Previous reports on organic nanowire systems have demonstrated spin valve signal only at low temperatures (< 100K) with a spin relaxation length of ~5 nm in Alq₃ [20], [25], [55] and ~47 nm in rubrene [56]. Single [57]–[60] and array-based [61], [62] carbon nanotube spin valves were also

reported, though the spin valve signal was present only at low temperature. In this work we investigate a new class of molecular nanotubes in which PCBM ([6,6]-phenyl-C₆₁-butyric acid methyl ester) molecules are held together via weak van der Waal's forces to form the tubular structure. PCBM has several inherent advantages over other organics. For example, PCBM is a soluble *fullerene* derivative, which is particularly attractive for bottom-up synthesis of solution-processable and printable organic devices. Fullerene and its derivatives are attractive for spintronics [52], [63]–[65] since these materials have weaker hyperfine interaction due to relatively less number of hydrogen atoms per molecule, as compared to other organics such as rubrene and Alq₃. This can lower the effect of hyperfine interaction on spin relaxation. Additionally, according to a recent theoretical study, fullerene has smaller “spin admixture parameter” compared to Alq₃, which can also result in longer spin relaxation length [23], [66]. Compared to fullerene thin films [52], [63]–[65], little (if any) is known to date about the spin transport properties of PCBM. Further, higher solubility of PCBM in common organic solvents (as compared to fullerene) allows easier growth process, since our nanowire growth technique is essentially “solution-based” [1].

Plasmons are the coherent oscillations of free electrons at visible frequencies. By confining the dimensions of a material, as is done in the case of nanowires, we can couple these plasmons more strongly with incident or radiative photons, improving the efficiencies of devices such as OPVs and OLEDs.

Photovoltaics, and energy technologies in general, are one of the most important challenges society is facing today. Improving the efficiency and lowering the cost of production of solar cells will play a large role in future energy production and reducing our impact on the environment. Organic photovoltaics are expected to be one technology that allows us to achieve this goal. Using the novel deposition technique in Chapter 2, it will be possible to fabricate coaxial nanowires of donor and acceptor materials for integration in solar cells. The small diameter of these

nanowires will ensure highly interdigitated features allowing for efficient generation of excitons and collection of electron-hole pairs.

1.5 Work Completed to Date

There are several projects presented in part or in full in this thesis. Two that have already been completed (novel centrifuge assisted template wetting method and spin valve effect in PCBM nanotube arrays) have been published in various journals [1], [48], [67]. The other ongoing projects are presented in section 1.6.

1.5.1 Novel Centrifuge Assisted Template Wetting Method

There have been studies on template growth of organic nanowires fabricated by placing drops of organic molecular solution on the surface of the template or by dipping the template in a beaker of the solution, also known as “template wetting” or the “dip and dry” method respectively [5], [68]. The solution enters the pores but once the solvent evaporates, all that is left is organic material. Typically this has been demonstrated on templates with through pores. A small number of studies on closed pore templates exist but those only report polymer nanowire formation, not small molecule nanowires [68]. Furthermore, in our experience this method has not successfully fabricated organic small molecular nanowires due to air pockets at the bottom of the pore, capillary and surface tension forces preventing solution from entering the pores.

A new deposition technique has been developed in this thesis that has many of the benefits of the above mentioned techniques with little draw backs. It is similar to the template wetting method but uses the assistance of a centrifuge to allow the solution to enter the pores. The technique is described later in detail (Chapter 2) but in short a porous AAO template is placed at the bottom of a centrifuge test tube and filled with a solution of organic small molecule dissolved in appropriate solvent. When the test tube is under centrifugal force, the solution inside is forced to the pore bottom where the organic molecules will remain after the solvent has evaporated.

1.5.2 Spin Valve Effect in PCBM Nanotube Arrays

To investigate spin transport properties of organic materials, a device known as a spin valve is commonly used, which sandwiches the material of interest between two ferromagnetic electrodes [17]–[19], [69], [70]. Typically a thin film of the material is used to construct the device. However, we have used an array of vertically aligned PCBM nanowires to connect the two electrodes to each other.

At this point in time, we have completed the majority of this project, although improvements can still be made. We have completed the fabrication of the final device as well as performed a range of measurements and characterization on it. Aluminum film anodization, Co nanowire electrodeposition, PCBM nanotube deposition and Ni thin film sputtering have all been successfully optimized as they are the fabrication steps for completing the device. Measurements and characterizations such as field emission scanning electron microscopy (FESEM) images, current-voltage (I-V) measurements, magnetoresistance (MR) responses, X-ray diffraction (XRD) and Raman spectroscopy have been performed to examine the device and verify its operation. Key results from this device that are presented in detail in Chapter 3 include a very large spin diffusion length (~50 nm) that persists even at room temperature, supporting the notion that PCBM is a strong candidate for spintronic applications.

1.6 Future and Ongoing Work

More work can be done on our spin valve device to obtain a stronger spin valve signal. As described in more detail in Chapter 4, changes in the device that could lead to such improvements could be shortening the length of the PCBM nanotube or improving the junctions between the PCBM nanotube and the ferromagnetic metal contacts.

A project that involves fabrication of metal-organic hybrid nanowire array on glass substrates for application in metamaterial and optoelectronic devices is currently in progress. At this point, anodization of an Al/Au/TiO₂ multilayer system on glass has been successfully optimized with two different electrolyte acids (3% oxalic acid and 0.3 M sulfuric acid). We have also successfully

deposited silver nanowires in the pores of these templates and are currently working to obtain device dimensions that exhibit resonant peaks at specific wavelengths and angles of incidents. Objectives that still need to be accomplished regarding the hybrid nanowire project include obtaining a longitudinal resonance in silver nanowires, obtain FESEM images of successfully grown organic nanowires in the templates on glass and the combination of successfully grown metal-organic hybrid nanowires and the characterization of these devices.

A future potential project, as briefly mentioned in section 1.4, is to apply the newly developed deposition technique to create an organic nanowire based photovoltaic device. One inherent property of the template based fabrication technique is that it forms tubes with a hollow center. Using PCBM as we have done will suffice as an acceptor material. This can then be used as a second template for a donor material such as poly(3-hexylthiophene-2,5-diyl) (P3HT). The final structure will be two coaxial nanowires with a radially oriented heterojunction of very high surface area. These characteristics should lead to high power conversion efficiencies.

Chapter 2. Nanoporous AAO Template Fabrication, Organic Nanowire Growth and Device Production Process Flow²

2.1 Summary

π -conjugated molecular organics such as rubrene, Alq₃, fullerene, and PCBM have been used extensively over the last few decades in numerous organic electronic devices, including solar cells, thin-film transistors, and large-area, low-cost flexible displays. Rubrene and Alq₃ have emerged as promising platforms for spin-based classical and quantum information processing, which has triggered significant research activity in the relatively new area of organic spintronics. Synthesis of these materials in a nanowire geometry, with feature sizes in the sub-100 nm regime, is desirable as it often enhances device performance and is essential for development of high-density molecular electronic devices. However, fabrication techniques that meet this stringent size constraint are still largely underdeveloped. Here, a novel, versatile, and reagentless method that enables growth of nanowire arrays of the above-mentioned organics in the cylindrical nanopores of anodic aluminum oxide (AAO) templates is demonstrated. This method 1) allows synthesis of high-density organic nanowire arrays on arbitrary substrates, 2) provides electrical access to the nanowire arrays, 3) offers tunability of the array geometry in a range overlapping with the relevant physical length scales of many organic devices, and 4) can potentially be extended to synthesize axially and radially heterostructured organic nanowires.

2.2 Background

A template-assisted method is commonly used for the fabrication of vertically oriented nanowire arrays [71]–[73]. This method allows straightforward fabrication of complex nanowire geometries such as an axially [1], [20], [56] or radially [74] heterostructured nanowire superlattice, which are often desirable in various electronic and optical applications. In addition, this is a low-cost, bottom-

² Portions of this chapter have been published in refs [1], [48]

up nanosynthesis method with high throughput and versatility. As a result, template-directed methods have gained immense popularity among researchers worldwide [72], [73].

The basic idea of the “template-directed method” is as follows. First a template is fabricated, which contains an array of vertically oriented cylindrical nanopores. Next, the desired material is deposited within the nanopores until the pores are filled. As a result the desired material adopts the pore morphology and forms a nanowire array hosted within the template. Finally, depending on the target application, the host template may be removed. However, this also destroys the vertical order. The geometry and dimensions of the final nanostructures mimic the pore morphology and hence synthesis of the host template is a critical part of the fabrication process.

Various types of nanoporous templates have been reported in literature [6]. The most commonly used templates include (a) polymer track-etched membranes, (b) block copolymers and (c) anodic aluminum oxide (AAO) templates. To create the polymer track etched membranes a polymer foil is irradiated with high-energy ions, which completely penetrate the foil and leave latent ion tracks within the bulk foil [49]. The tracks are then selectively etched to create nanosized channels within the polymer foil [49]. The nanosized channels can be further widened by a suitable etching step. Key problems with this method are the non-uniformity of the nanochannels, lack of control of location, non-uniform relative distance between the channels, low density (number of channels per unit area $\sim 10^8/\text{cm}^2$), and poorly ordered porous structure [71]. In the block copolymer method a similar cylindrical nanoporous template is first created, followed by the growth of desired material within the pores [6].

In the past, methods (a) and (b) mentioned above have been used to fabricate polymer nanowires [6]. However, these methods may not be suitable for synthesizing nanowires of any arbitrary organic material due to the potential absence of selective etching during post-processing steps. Post-processing typically involves removal of the host template, which for the above-mentioned

templates would require organic solvents. Such solvents may have deleterious effect on the structural and physical properties of the organic nanowires. However, these templates work as ideal hosts for inorganic nanowires such as cobalt [75], nickel, copper and metallic multilayers [47], which remain unaffected in the etching process that removes the polymer host. Another potential challenge for the above-mentioned methods is the poor thermal stability of the host matrix at higher temperatures. High temperature annealing is often required to improve crystallinity of the organic nanowires, which indicates the necessity of good thermal stability of the host matrix.

Controlled electrochemical oxidation of aluminum (also known as “anodization” of aluminum) is a well-known industrial process and is commonly used in the automobile, cookware, aerospace and other industries to protect aluminum surface from corrosion [76]. The nature of the oxidized aluminum (or “anodic alumina”) depends critically on the pH of the electrolyte used for anodization. For corrosion-resistance applications, anodization is generally performed with weak acids (pH ~ 5-7), which create a compact, non-porous, “barrier-type” alumina film [76]. However, if the electrolyte is strongly acidic (pH < 4), the oxide becomes “porous” due to local dissolution of the oxide by the H⁺ ions. The local electric field across the oxide determines the local concentration of the H⁺ ions and hence surface pre-patterning prior to anodization offers some control over the final porous structure. The pores are cylindrical, with small diameter (~ 10-200 nm) and hence such nanoporous anodic alumina films have been used extensively in recent years for synthesizing nanowires of various materials [72], [73].

Nanoporous anodic alumina templates offer better thermal stability, high pore density, long-range pore order, and excellent tunability of pore diameter, length, inter-pore separation and pore density via judicious choice of anodization parameters such as pH of the electrolyte and anodization voltage [72], [73]. Due to these reasons we choose AAO templates as the host matrix for the organic nanowire growth. Further, inorganic oxides such as alumina have high surface energy, thus facilitating uniform spreading of the organic solution (low surface

energy) on the alumina surface [77]. In addition, our goal is to grow these nanowire arrays directly on a conductive and/or transparent substrate. As a result, the pore is closed at the bottom end, which needs additional consideration as we describe below. Growth of nanowires within a through-pore template and subsequent transfer to the desired substrate is often undesirable due to poor interface quality and this method is not even feasible for short-length nanowires (or thin templates) due to poor mechanical stability of the thin templates.

π -conjugated organic materials can be broadly classified into two categories: (a) long-chain conjugated polymers and (b) small molecular weight organic semiconductors. Many groups have reported synthesis of long chain polymer nanowires within the cylindrical nanopores of an AAO template in the past. Comprehensive review on this topic is available in refs [6], [68]. However, synthesis of nanowires of commercially important small molecular organics (such as rubrene, tris-8-hydroxyquinoline aluminum (Alq_3), and PCBM) in AAO is extremely rare. Physical vapor deposition of rubrene and Alq_3 within the nanopores of AAO template has been reported by several groups [20], [25], [55], [78]. However, only a thin layer (~ 30 nm) of organics can be deposited within the pores (~ 50 nm diameter) and prolonged deposition tends to block the pore entrance [20], [25], [55]. Complete pore filling can be achieved in this method if the pore diameter is sufficiently large (~ 200 nm) [78]. Thus it is important to find an alternative method that is applicable for pore diameters in the sub-100 nm range.

Another approach that has been used for some other small-molecular organics is a so-called “template wetting” method [6], [68]. However, in most reports thick commercial templates (~ 50 μm) with both side open pores and large diameter (~ 200 nm) have been used [79], [80]. Such method has not produced nanowires in one-side closed pores as mentioned before, presumably due to the presence of trapped air pockets within the pores, which prevents infiltration of the solution within the pores. In this chapter we report a novel method developed by us that overcomes these challenges and allows growth of small molecular organic

nanowire arrays with arbitrary dimensions on any desired substrate. In what follows, we will describe the detailed protocol, potential limitations and future modifications.

2.3 Fabrication Protocol

As mentioned above, the two key steps in the AAO-based fabrication process are (a) synthesis of the empty AAO template on arbitrary (primarily conductive and/or transparent) substrates (schematic description in Figure 2.1) and (b) growth of desired materials (metals, small molecular organics etc.) nanowires within the nanopores of the AAO template. In this section we provide a detailed description of these processes.

1) Growth of Anodic Aluminum Oxide (AAO) Templates on Conductive Aluminum Substrates.

1.1) Nanoporous alumina templates are created by first polishing aluminum foils and then anodizing (or electrochemically oxidizing) them. We begin by cutting out small (~ 2 cm x 2 cm) sheets of high purity unpolished aluminum (99.997%, Alfa Aesar) with thickness 250 μm .

1.2) In lieu of electropolishing, a simpler chemical polishing process [81] is used. We submerge 2 cm x 2 cm Al sheets in nitric-phosphoric acid etchant at 80 °C on a hotplate for 5 minutes. The nitric-phosphoric acid solution used to pre-treat the aluminum sheets is 15 parts 68% nitric acid and 85 parts 85% phosphoric acid. A polishing step is necessary prior to anodization because surface roughness of as-purchased aluminum is of the order of few microns, which creates non-uniform electric field at the surface and prevents formation of ordered pore array. In literature, electropolishing has been used extensively for this purpose [72], [73]. However, chemical polishing is a cheap and easy alternative, which also yields polished surfaces with comparable (or better) smoothness [81].

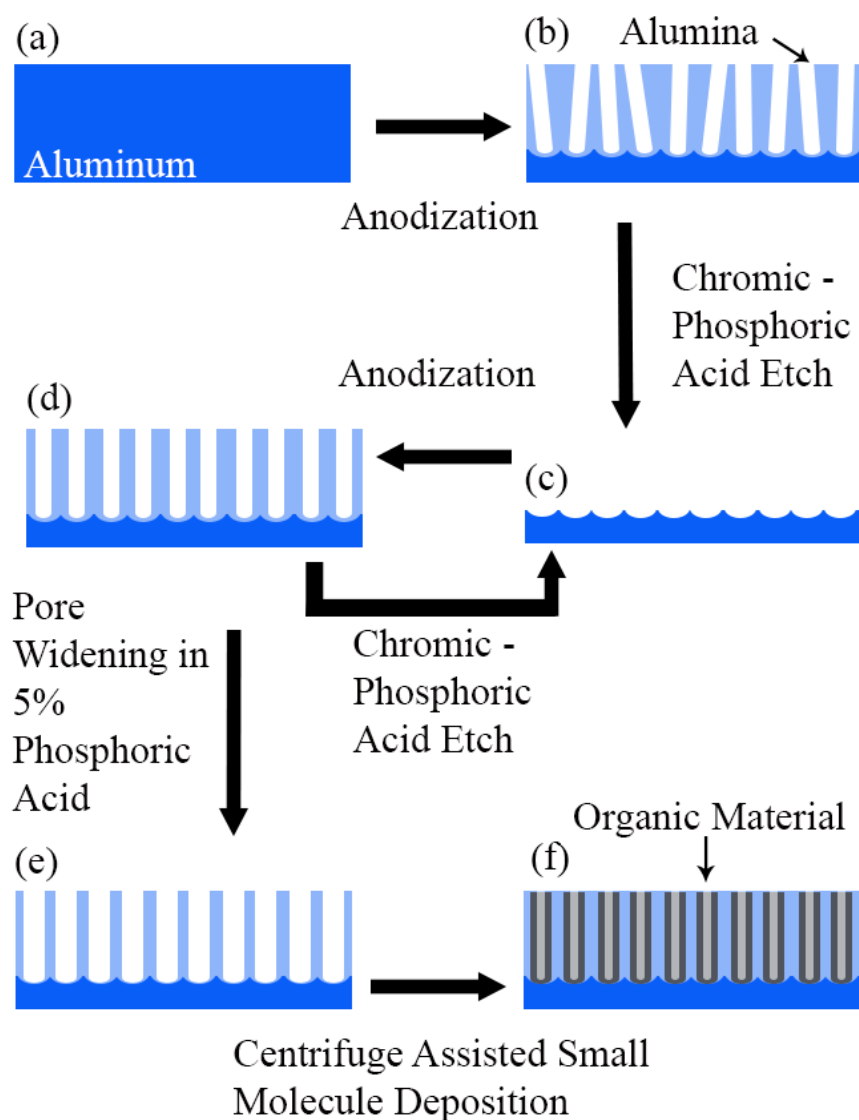


Figure 2.1 Schematic description of the organic nanowire synthesis. Steps (a) – (e) represents multi-step anodization and etching for fabrication of well-ordered nanopores. Step (f) represents organic nanowire growth.

1.3) After etching, we neutralize the foils in 1 M sodium hydroxide for 20 minutes. These “chemically polished” foils are now ready to be anodized.

1.4) We load the polished aluminum sheets in to flat cells and anodize them for 15 minutes with 3% oxalic acid at 40 V DC bias. For foil samples a two-step anodization process is performed to improve pore ordering [72], [73], [82]. This

first step will create a porous oxide layer on the Al surface and nano-scale dimples at the aluminum/alumina interface, which act as the initiation sites for pore growth during second step of anodization.

1.5) We etch the sample in chromic-phosphoric acid by removing it from the flat cell. We immerse the sample in a beaker of the etchant on a hot plate at 60 °C for ~30 minutes to remove the initial oxide layer.

1.6) We repeat the anodization process (step 1.4) for 2.5 minutes while keeping all other parameters unchanged. It is important to realign the foil in the flat cell such that the same area anodized in step (1.4) will again be exposed to the electrolyte. The time of the final anodization step determines the thickness of the final oxide layer and can be altered accordingly. Duration of 2.5 min. corresponds to a film thickness (pore length) of ~500 nm. At the end of the second step a well-ordered nanopore array is created in the anodic alumina layer. The anodization and etching cycle can be repeated to further improve pore ordering.

1.7) Finally we submerge the template in 5% phosphoric acid at room temperature for 40 minutes to thin the barrier layer at the bottom of the nanopores and widen the nanopore diameter. Final nanopore diameter after this step is ~ 60-70 nm. Figure 2.2 shows the resulting empty template.

2) Growth of AAO Templates on Transparent Substrates (Glass).

2.1) We deposit the following multilayer system sequentially on cleaned glass slides: TiO₂ (20 nm, atomic layer deposition), Au (7 nm, sputtering), Al (700 nm, sputtering). Deposition parameters are as follows:

TiO₂: 350 Cycles of plasma enhanced ALD at 3 Watts (0.51 Å/cycle) with the precursor Ti(OC₃H₇)₄ and a table temperature of 200 °C.

Au: 30 seconds at 80 Watts (14.2 nm/min)

Al: 52 min at 300 Watts (13.4 nm/min)

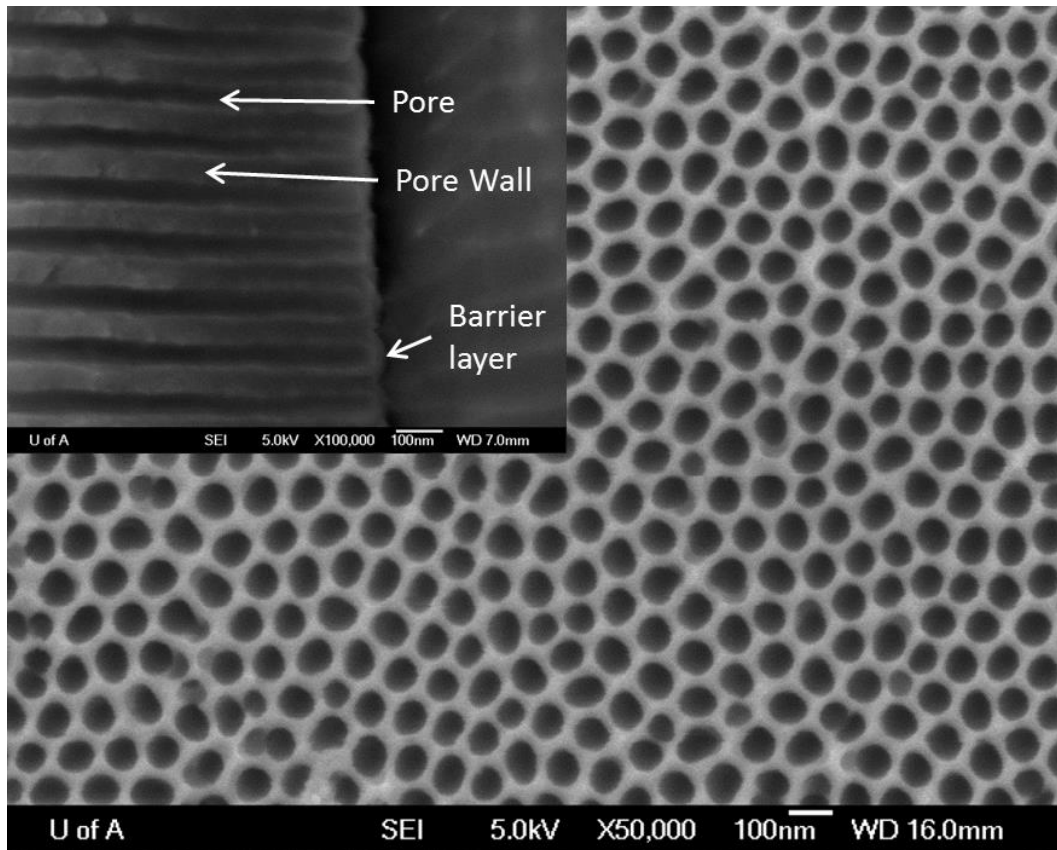


Figure 2.2 FESEM image of empty template anodized on Al foil. Main image shows pore structure while inset shows a cross section of the pores with barrier layer present at bottom.

The Au layer acts as an electrode, required for anodization, and does not deteriorate transparency [83]. The TiO_2 acts as a transparent adhesion layer between the Au and glass substrate.

2.2) We attach a foil electrode to the surface of the thin film of aluminum to be anodized using a conductive silver epoxy. This will result in a proper connection from power source to sample while improving current distribution. Since there is very little aluminum deposited on the glass substrate, polishing techniques mentioned before are not viable to flatten the aluminum surface. Instead we modify the anodization procedure to incorporate another anodization/etching step.

2.3) We load the sample in to the flat cell and anodize the aluminum thin film for 4 minutes using 3% oxalic acid at 30 V DC bias.

2.4) Without removing the sample from the flat cell, we rinse the cell out with deionized (DI) water and etch the template in chromic-phosphoric acid at 60 °C for 1 hour by pouring the hot etchant in to the cell.

Note: The temperature of the etchant will immediately start to decrease once it has been poured in to the cell. Therefore, the duration of etching is increased to 1 hour from 30 minutes for the foil samples to ensure all oxidized film is removed.

2.5) We rinse out the cell again and anodize a second time under the same conditions as the first; for 4 minutes, using 3% oxalic acid at 30 V DC bias.

2.6) We repeat step (2.4). Without removing the sample from the flat cell, we rinse the cell out with DI water and etch the template in chromic-phosphoric acid at 60 °C for 1 hour by pouring the hot etchant in to the cell.

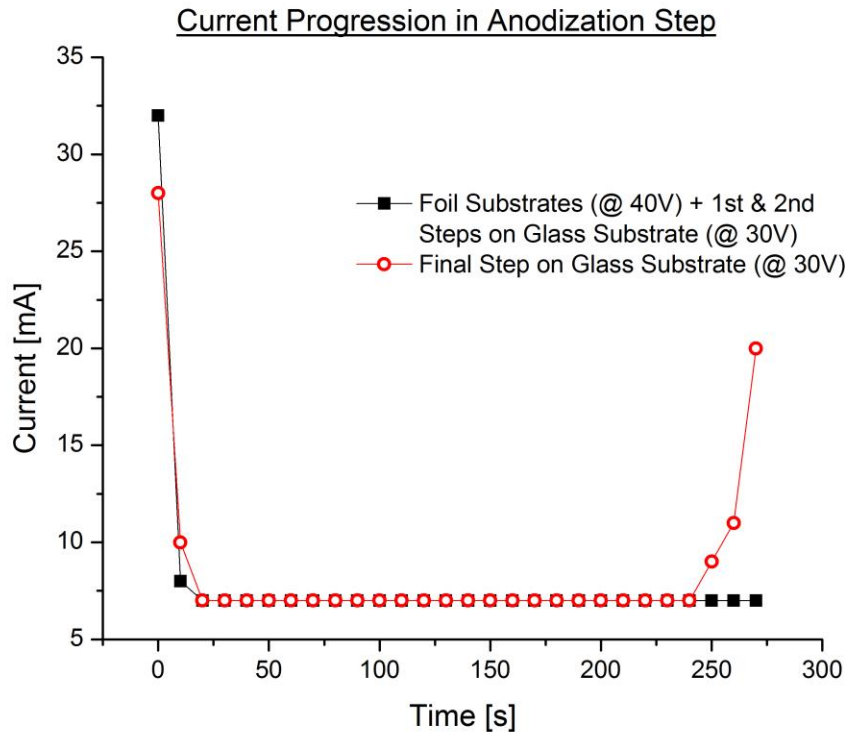


Figure 2.3 Anodization current as a function of time. For the final step of anodization on glass substrate, current rises when the entire aluminum is consumed and the electrolyte comes in contact with the underlying Au layer.

2.7) We rinse the cell out for the final time and perform the third (and last) anodization step, using 3% oxalic acid at 30 V DC. We monitor the current of the system to determine when to stop. The current needs to be monitored during the final anodization. After the first few seconds, the current stabilizes at around 1-2 mA. This indicates uniform anodization is taking place. Once the anodization process has consumed the remaining aluminum, the electrolyte solution (3% oxalic acid) will come in to contact with the underlying gold layer, which will cause a sharp increase in the anodization current (Figure 2.3). At this point, the anodization is stopped. The time should be roughly around the 4 minute mark. This rise in current is not observed in foil samples (Figure 2.3) because the aluminum is never fully consumed and a uniform barrier layer separates the solution and metal substrate.

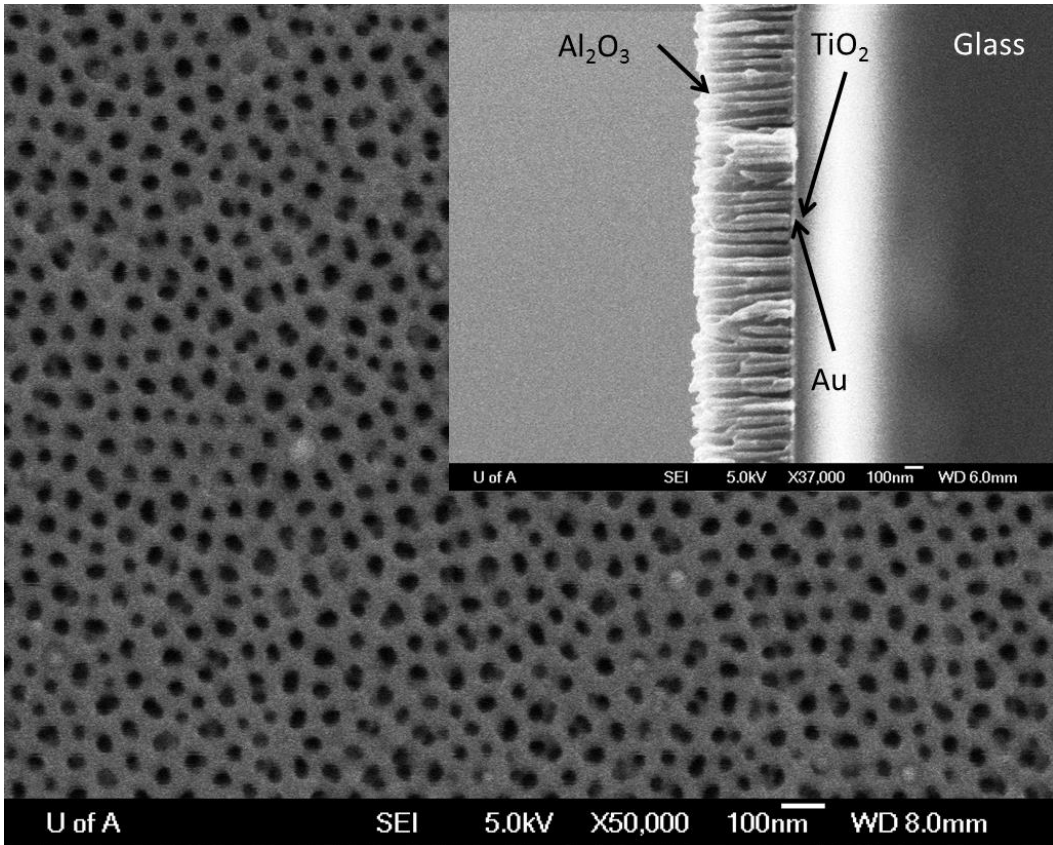


Figure 2.4 FESEM image of empty template anodized on Al thin film on glass. Main image shows pore structure while inset shows a cross section of the pores with layered structure (500 nm porous Al₂O₃ / 7 nm Au / 20 nm TiO₂ / glass substrate).

2.8) We perform a pore widening step, similar to the foil sample protocol by submerging the template in 5% phosphoric acid at room temperature for 40 minutes. This will widen the pores but since the anodization process has eaten through the barrier layer there is none left to thin. Figure 2.4 shows the layered structure of glass substrate / 20 nm TiO₂ / 7 nm Au / 500 nm porous Al₂O₃ with the absence of a barrier layer and pores clearly exposed to underlying Au thin film.

3) Centrifuge-Assisted Growth of Small Molecular Organic Nanowires Within the Pores of AAO Template.

3.1) We prepare a saturated solution of the small molecular organic in a suitable solvent. The following organic molecules and solvents have been used: rubrene in acetone, Alq₃ in chloroform and PCBM in toluene. From here on we will refer to PCBM as the molecule of interest.

3.2) We load the templates in to the bottom of a centrifuge test tube such that the anodized area is facing the top of the test tube. The tube must be large enough to fit the sample inside. For foil samples, it is helpful to use a wafer of similar size to support the foil and prevent bending during centrifugation as described below. Figure 2.5 shows a schematic description of how the sample is mounted in the centrifuge.

3.3) We use a pipette to fill the test tube with enough PCBM solution such that the template is completely submerged.

3.4) We load the test tube in the centrifuge and run for 5 minutes at 6000 rpm. If the samples were mounted in the test tube at an angle, we ensure the test tube is mounted in such a way that the anodized surface is pointing towards the center of the centrifuge (Figure 2.5).

3.5) Once the centrifuge has stopped, we unload the test tubes and pour out the PCBM solution from them back in to the organic solution bottle.

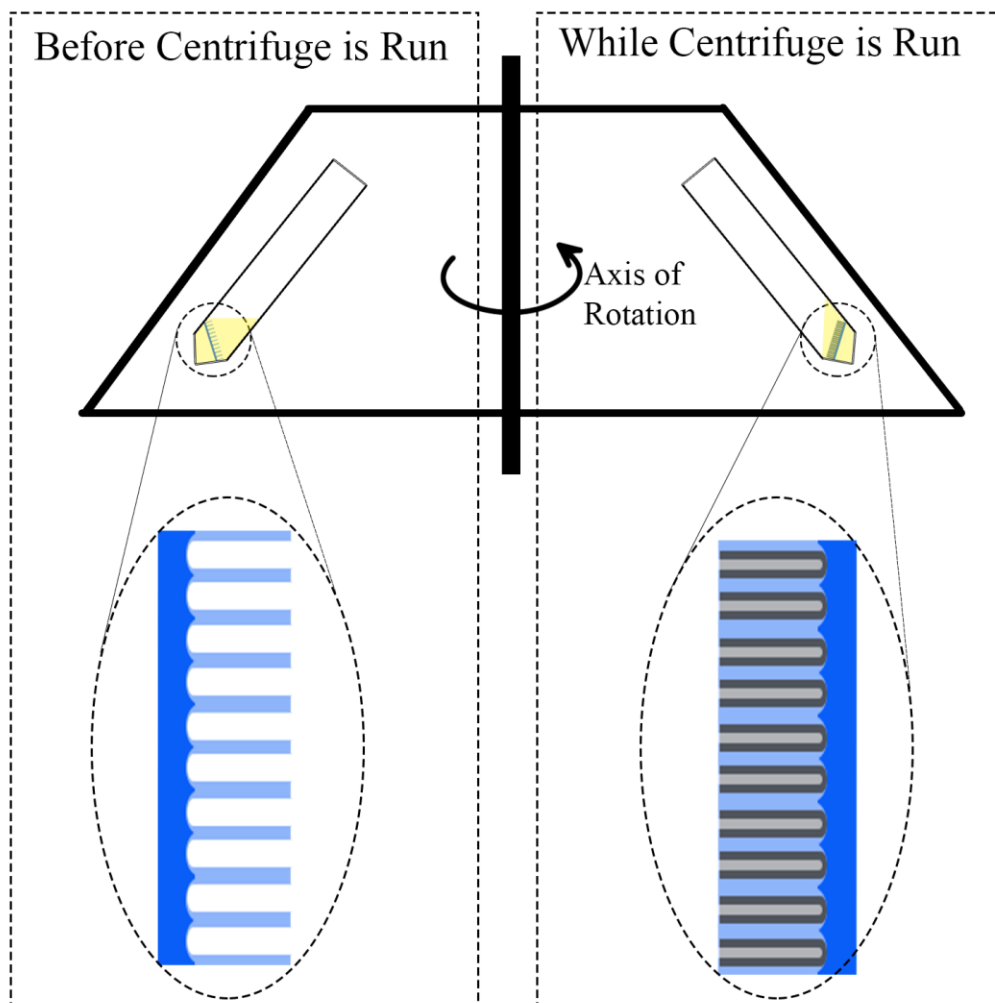


Figure 2.5 Schematic of the centrifuge and loading of the empty template in the test tube for organic nanowire growth.

3.6) We remove the templates from the test tubes, or leave them at the bottom, for ~ 1 minute to dry.

3.7) We repeat steps 3.2 – 3.6 so that a total of 5 – 10 centrifuge runs have been performed. In situations where there is low solubility of the small molecule in its solvent, more centrifuge runs will help deposit more material in the nanopores.

3.8) We remove the sample from the bottom of the test tube and use a cotton swab soaked in toluene (or the respective solvent) to gently clean the surface of the template, removing any material that is left over on the surface of the template.

Figure 2.6 shows the resulting PCBM nanowires occupying the void of the empty pores.

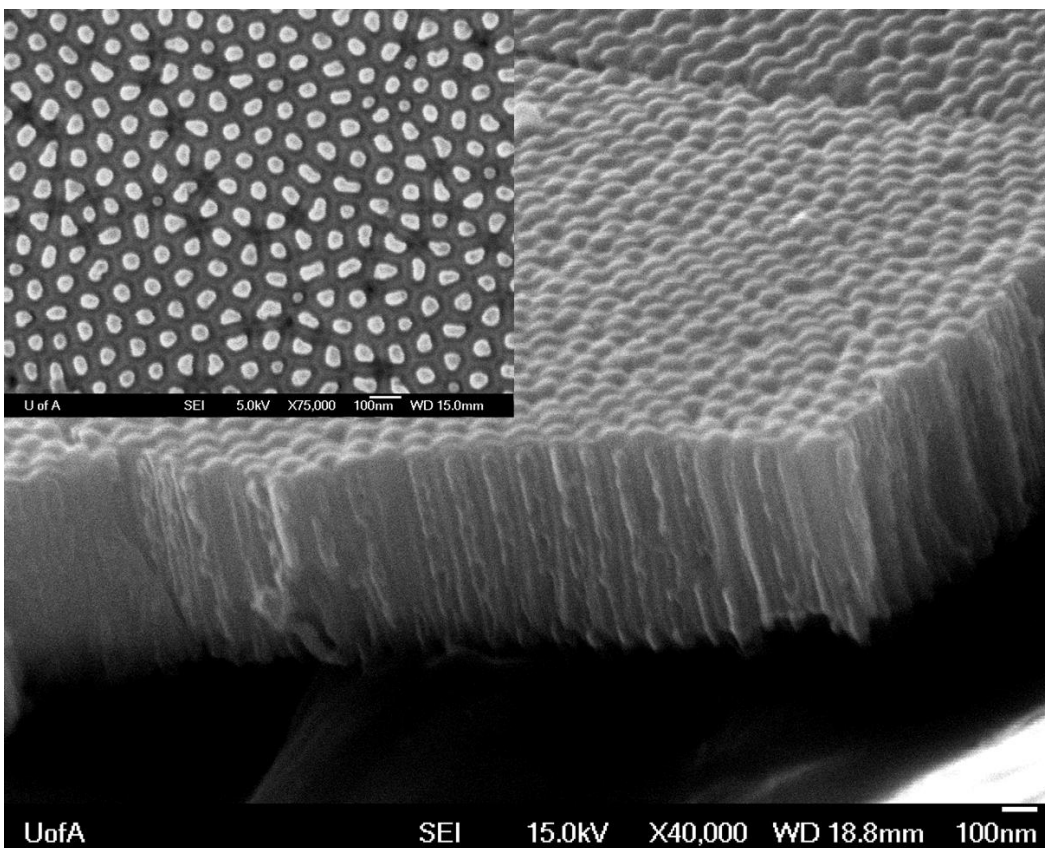


Figure 2.6 FESEM of PCBM nanotubes. Main image shows a cross section of the template with the entire length of the pore filled with PCBM, displaying the hollow nature of the tubes. Inset is a normal view of the bottom side of the template after the barrier layer has been removed. This shows a capped end to the nanotube.

4) Electrochemical Deposition of Metallic Nanowires Within the Pores of AAO Template.

4.1) We prepare a solution containing the metallic ion of interest (i.e. AgNO_3 for silver nanowire growth or CoSO_4 for cobalt nanowire growth). For simplicity, we will refer to cobalt as the material of interest going forward. Many other metals can be used to fabricate nanowires in this method (Au, Ni, Cu etc.) however only Ag and Co were used in this thesis. These metallic nanowires are needed for the fabrication of organic nanowire spin valves and metal-organic hybrid nanowires for optical applications.

4.2) After anodization, there is a clearly defined 1 cm diameter circle on the substrate. This circle is the porous alumina film. To ensure electro-deposition occurs in the pore bottoms and not around the edges of the film (which can be the result of imperfect alignment in the flat cell) an insulating epoxy is applied to the rim of the film, slightly overlapping with the film itself.

4.3) We load the sample in to the flat cell such that the uncovered portion of the film is fully exposed in the opening to the cell.

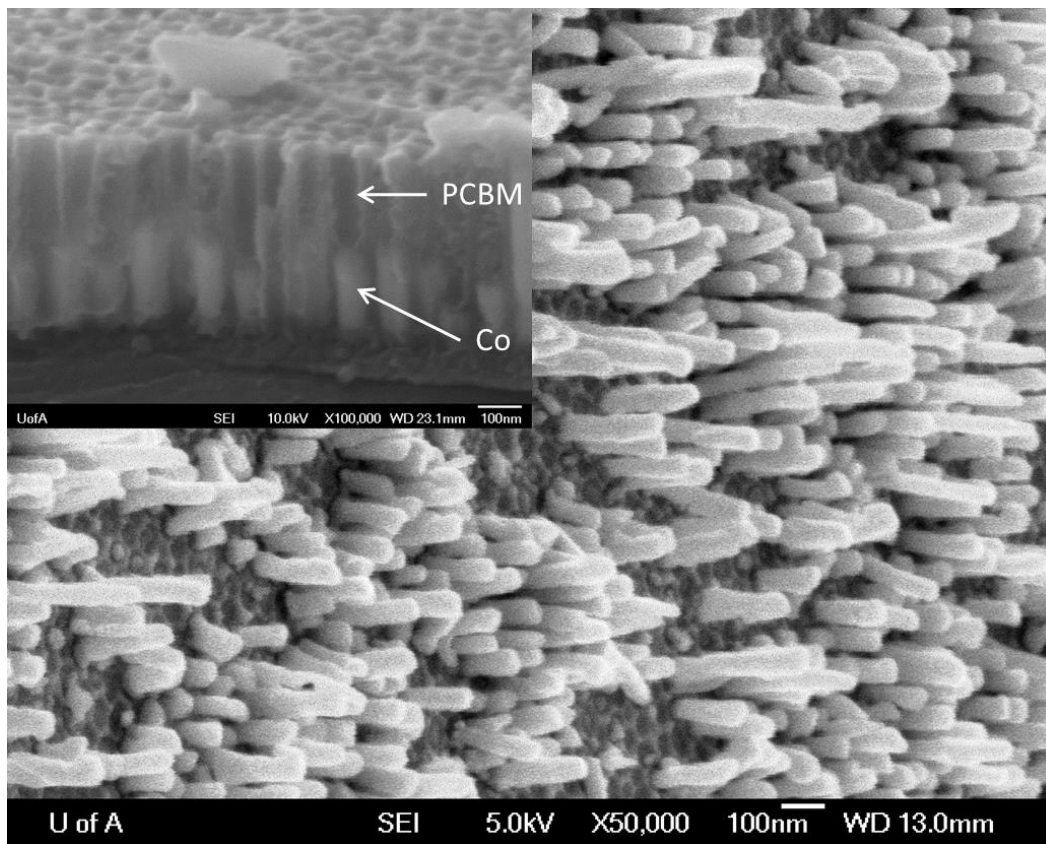


Figure 2.7 FESEM of metallic nanowires grown inside AAO template. Main image is of a field of Ag nanowires grown in AAO template on glass after the matrix has been removed. Inset is a cross section of Co nanowires grown in the pores of AAO on foil substrate with PCBM nanotubes grown on top.

4.4) We fill the cell with the CoSO_4 solution and electrodeposit at 20 V AC and 250 Hz. The duration of deposition can be varied to produce nanowires of different length, useful for different applications. Current progression should fall

immediately from a large value (few hundred mA) to a low value (~2 mA) and stabilize for the duration of deposition. The current should be closely monitored as this is an indication of uniformity and length. Once the entire length of the pore is filled with metal, it will begin to “overflow” with material causing a jump in the current.

4.5) We remove the power source after 1 minute of electro-deposition. This will result in Co nanowires of ~ 200 nm. The duration of electro-deposition can be varied to produce nanowires of different lengths. This can have an impact on the performance of various devices.

5) Sputtering of Thin Film Contacts.

5.1) Using double-sided carbon tape, we mount the sample to a 4 inch Si wafer. This will allow the sample to be mounted in the vacuum chamber.

5.2) We wrap the Si wafer in aluminum foil and mark the location of the sample in the foil. This aluminum foil wrap will act as a mask for the deposition process.

5.3) We remove the foil from the wafer and using tweezers, punch out small holes in the foil where the sample will sit. The location of these holes will determine the location of the contacts on the sample.

5.4) We mount the sample in the deposition chamber and deposit ~80 nm of metal (depending on the application) to act as the top contact for the organic device. This metal can be a ferromagnetic metal (Ni) or non-magnetic metal (Ag).

2.4 Discussion on Centrifuge Assisted Template Nanowire Growth

2.4.1 Physical Picture for Nanowire Growth

It is important to develop a physical understanding of the growth method of the organic nanowires. Once we know exactly how they grow and form themselves in the pores we can use this deposition method to engineer nanostructures, devices and materials. In the past, polymer nanowires have been fabricated using the

template wetting procedure without the assistance of a centrifuge, but for some materials such as organic small molecules, we have found this to be ineffective [84]. Due to surface chemistry between the solution and template as well as the air pocket trapped in the nanopore, the solution is unable to freely enter the pore. When the solution is under the influence of the centrifuge's centrifugal force, it is in essence adding to the gravitational force the sample was already experiencing. Because the organic solution is obviously denser than the air occupying the pore it is forced to the pore bottom under the increased centrifugal force. Once the solution has overcome the forces keeping it from naturally entering the pores, it will continue to occupy the pore even after the centrifuge is stopped. The sample is then removed from the centrifuge and left out to dry. Because organic solvents evaporate relatively fast, the drying process only takes about a minute at room temperature. The solution in the pore nearest to the pore opening will evaporate first and progress lower and lower until the solution at the pore bottom has evaporated and all that is left in the pore is the organic small molecules. As the solution evaporates and exits the pore nearest to the pore opening, the small molecules that were dissolved in that volume of solvent get pushed to the pore walls and remain there under van der Waals forces. The solvent continues to evaporate down the length of the pore continually depositing material on the pore walls through the entire length of the pore, creating a continuous and hollow nanotube inside the pore. Once this process reaches the pore bottom, there will be a slight excess of small molecules, which will coat the pore walls at the bottom as well as the barrier layer at the pore bottom. This will create a "capped" end to the nanotube at the pore bottom that can be very beneficial to devices needing proper electrical contact to the nanotube material. Repeated centrifugation will result in solid nanowires instead of hollow nanotubes.

2.4.2 Critical Parameters

One critical parameter that needs to be considered in the deposition process is the RPM of the centrifuge. If the RPM is too low, the centrifugal force will not be strong enough to replace the trapped air pockets with organic solution. For most centrifuge setups, the maximum RPM setting should be able to be used. As long

as foil substrate samples are supported with a strong enough backing (wafer, glass or other substrate), there should be no mechanical damage done to the template even in conical shaped centrifuge tubes.

The concentration of the small molecule in the solvent of choice is also an important factor in the process. The more soluble a material is in its solvent, the more material will be deposited in the pore. For most applications, researchers should use a saturated solution of the material in solvent to maximize the amount of material in the pore. However, one should theoretically be able to control the wall thickness of the nanotube by manipulating the solution concentration. A lower concentration would limit the number of molecules available to form a tube and result in a thinner tube wall.

Run time or length of centrifugation is another parameter we can control. This parameter does affect the final structure that is formed. Run time needs to be long enough to ensure all pores have been filled with solution, which could be different for different setups (solvent and template combinations). For our particular setup, we have found that run times of 5 minutes will suffice. For solutions that have low solubility in solvents, we can repeat the deposition procedure a few times. The more centrifuge runs we perform, the more material there should be deposited in the pore. Increasing the number of runs can help deposit more material in the pores and increase the chances of nanotube formation in low concentration solutions.

Anodization on aluminum foils has been explored extensively and is a well-known process [72], [73]. While anodization on glass is nothing fundamentally new, it is less developed than foil anodization and incorporates more challenges. Due to the thin gold electrode, a high current density can result when the aluminum is completely anodized and the acid comes in contact with the electrode (Figure 2.3). It is important to keep the voltage at a level lower than that of foil anodization to avoid pore merging and overheating/burning of the alumina template.

2.4.3 Potential Benefits and Drawbacks

The main benefits this centrifuge-assisted technique has over other forms of organic small molecule deposition are that it is low-cost, simple and does not require any complex experimental setup. The only equipment needed for this technique is a centrifuge, which is relatively inexpensive and readily available in most nanofabrication facilities when compared with complex vacuum chambers, pumps and power sources needed for evaporation of organic materials in PVD techniques. This technique also allows for extremely high aspect ratio features to be deposited in and features where there is not a direct line of sight from crucible or source material to the location of deposition, which is needed in all PVD type deposition techniques. It is also compatible with other solution processing techniques, which will become more and more common as organic electronic devices become more commercially viable.

While this is a new deposition technique that enables users to easily deposit organic molecules in to high aspect ratio features, it does have some drawbacks. Using this technique, we are limited to solution processable molecules. If the material does not have the ability to dissolve in some solvent, we will not have a carrier to transfer it in to the pore. Also, because this is a template fabrication technique, the limitations we encounter for producing the template will also limit the structures we can grow inside them. This technique does not have the ability to control nanowire length within the pore or vary any other parameter of the wire after template is grown. Once the template is formed, the entire length of the pore will be deposited in, which will determine the nanotube length. The final pore diameter will determine the nanotube diameter. However, fortunately the AAO template growth process is heavily investigated [72], [73] and enormous control over nanopore geometry is available, including the possibility of creating branched and modulated diameter pores [85]. Therefore this is presumably not a very serious limitation.

2.4.4 Future Directions, Modification and Potential Applications

This centrifuge-assisted method is a novel deposition technique with many features that need to be characterized and investigated. There is still a lot of work to do to determine the capabilities and limitations of this technique. To this point, only a fixed angle centrifuge has been used for deposition. This type of centrifuge makes mounting the substrate at the proper angle a challenge. One way to circumvent this problem is to use a variable angle centrifuge with flat bottom test tubes. As the centrifuge picks up speed, the arms of the centrifuge that hold the test tubes will swing out such that the centrifugal force will remain perpendicular to the flat bottom of the test tube. This will ensure that the solution will always be directed parallel to the pore length and that no component of the force will push the solution to the side of the template. Further work also needs to be done to better understand how manipulating the critical steps of the process affect the final structure. The effect of annealing on crystallinity should also be examined to better understand the physical properties of the resulting nanotubes.

In future, this versatile deposition technique may find application in diverse areas such as memory devices [86], [87], organic photovoltaics [9], [11], [13], [14], [88], [89], plasmonics [90], chemical sensors [91], [92], OLEDs [93] and organic nanowire FETs [15], [16]. Two structures that are currently being explored in our group are axially and radially heterostructured organic nanowire devices. We have already fabricated axially heterostructured metal-organic hybrid nanowire structures for applications in organic spintronics by electrodepositing metal nanowire in the bottom of the pore and filling the remaining portion with organics [1], [56], [67]. The work on fabricating coaxial organic nanowires is currently in progress and such structures are promising candidates for high-efficiency organic photovoltaic devices [9], [10], [94], [95]. Results of the electrical and spin transport measurements for the axially heterostructured devices will be discussed in Chapter 3.

Chapter 3. Magnetoresistance Study of PCBM Nanotube Spin Valves³

3.1 Summary

Organic spin valve array, with vertically oriented methanofullerene [6, 6]-phenyl C61- butyric acid methyl ester (PCBM) nanotubes as spacer, has been prepared by combining an electrochemical self-assembly with the fixed angle centrifuge-assisted organic nanowire growth technique described in Chapter 2. The PCBM nanotubes are ~ 325 nm long, have outer shell diameter of ~ 70 nm and inner shell diameter of ~ 45 nm. In spite of the relatively long channel length, these devices exhibit an inverse spin valve effect, which persists even at room temperature. Spin relaxation length in PCBM nanotubes is relatively temperature-independent and its lower limit is estimated to be ~ 50 nm at room temperature. This is the largest room-temperature spin relaxation length in organic nanowire systems, including carbon nanotubes reported to date, and identifies PCBM as a promising material for room temperature organic nanospintronics. Observation of spin valve signals in these devices is due to efficient spin selective transmission at the interfacial Schottky barriers.

3.2 Introduction

In recent years organic semiconductors have emerged as a promising platform for spintronics [17]–[19], [69], [70] since these materials permit chemical tunability of spin filtering [96]–[100] and spin relaxation [22], which are the two key processes in spintronics. Spin transport in organics has been mostly investigated by “organic spin valve” devices in which a layer of organic is sandwiched between two ferromagnetic electrodes [17]–[19], [69], [70]. Organic spin valves can be broadly divided into two categories [101], [102]: (1) *tunneling devices*, in which ultrathin organic layers are used as tunnel barriers (sometimes in conjunction with other inorganic tunnel barriers, such as alumina) [36], [100], [103] and (2) *injection devices*, in which carrier transport occurs via hopping

³ Portions of this chapter have been published in ref. [67]

between various molecular sites within a thick organic layer [20], [104]–[106]. For the former category, room temperature operation and large tunneling magnetoresistance has been demonstrated [36], [103]. For the latter category, spin signal becomes weaker with increasing thickness of the organic and operating temperature [105], [106]. In spite of the weaker spin valve signal, injection devices are expected to offer more insight into interaction of carrier spins with organic molecules, which results in spin relaxation. This process is still poorly understood in organics.

In this work, we find that in PCBM nanotubes with relatively large length of ~ 325 nm, the spin valve signal persists at room temperature. Spin valve signal has been found to be relatively independent of temperature. At room temperature the lower bound of spin relaxation length in PCBM nanotubes is ~ 50 nm, which is the largest *room-temperature* spin relaxation length in *nanowire* organic systems, *including carbon nanotubes*, reported to date. Further, we note that PCBM is extensively used in bulk-heterojunction solar cells and the ability to maintain well-defined spin polarizations at room temperature in this material can offer novel ways to improve the power conversion efficiency of such devices [107].

3.3 Device Fabrication

We fabricated [cobalt nanowire/PCBM nanotube/nickel] and [cobalt-nanowire/PCBM nanotube/alumina barrier/nickel] vertical spin valve arrays using a hybrid method that combines electrochemical self-assembly with the centrifuge assisted organic nanowire growth technique [1], [81] described in Chapter 2. A schematic diagram of the final spin valve device is shown in Figure 3.1. The PCBM nanotubes (NTs) are hosted within a nanoporous alumina template and are physically separated from each other by the insulating alumina host matrix (Figure 3.2). These nanotubes are contacted by cobalt nanowires at the bottom and nickel thin film (with or without an interfacial alumina barrier) at the top. Transition metal contacts have been chosen due to their large Curie temperature ($\gg 300\text{K}$), which ensures significant spin polarization of the contacts even at room temperature.

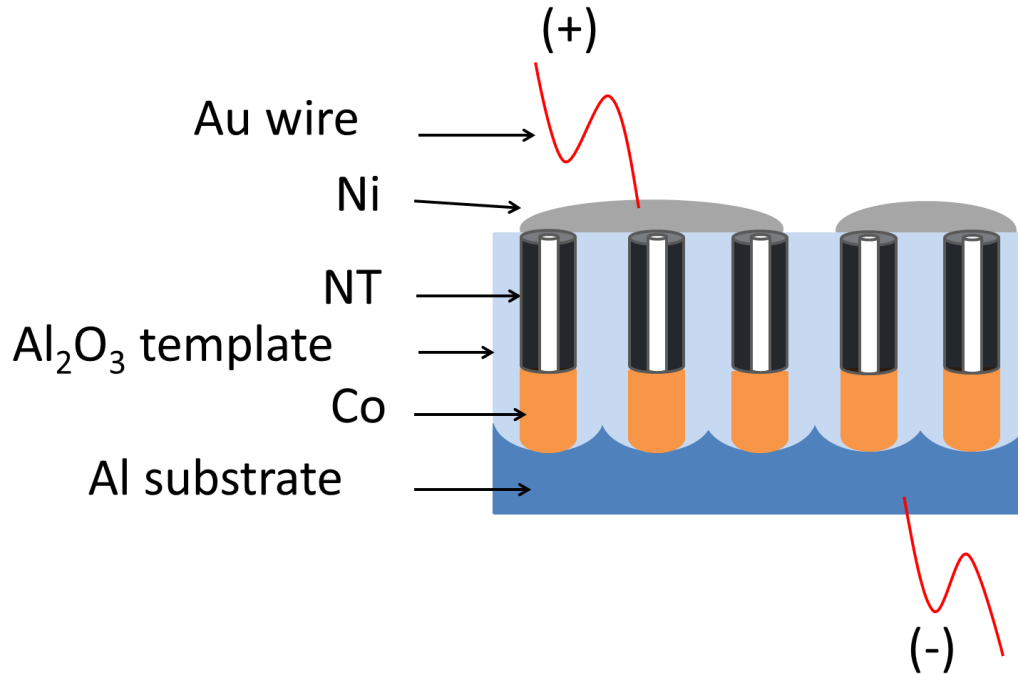


Figure 3.1 Schematic of final PCBM nanotube spin valve array device structure.

Interfacial barriers are widely used in organic spin valves (especially vertical geometry) since they serve multiple purposes: (a) circumventing the conductivity mismatch problem and improving the spin injection efficiency [36], [103], [108], (b) better quality ferromagnetic films are obtained when deposition is performed on alumina compared to soft organic [52] and (c) protecting the underlying organic from interdiffusion of ferromagnetic species during evaporation of the top contact [104], [105], thus leading to a well-defined top interface. In the present case, the e-beam evaporated nickel penetrates only < 10 nm near the top edge of the nanotubes and mostly resides on the top surface of the alumina template (Figure 3.3). As discussed later in this chapter, presence of an interfacial tunnel barrier between PCBM tubes and top Ni did not offer any significant improvement in the magnitude of the spin valve signal. This is consistent with previous studies that found fullerene-based systems to be more robust against the interdiffusion problem compared to other organics such as Alq₃ [63].

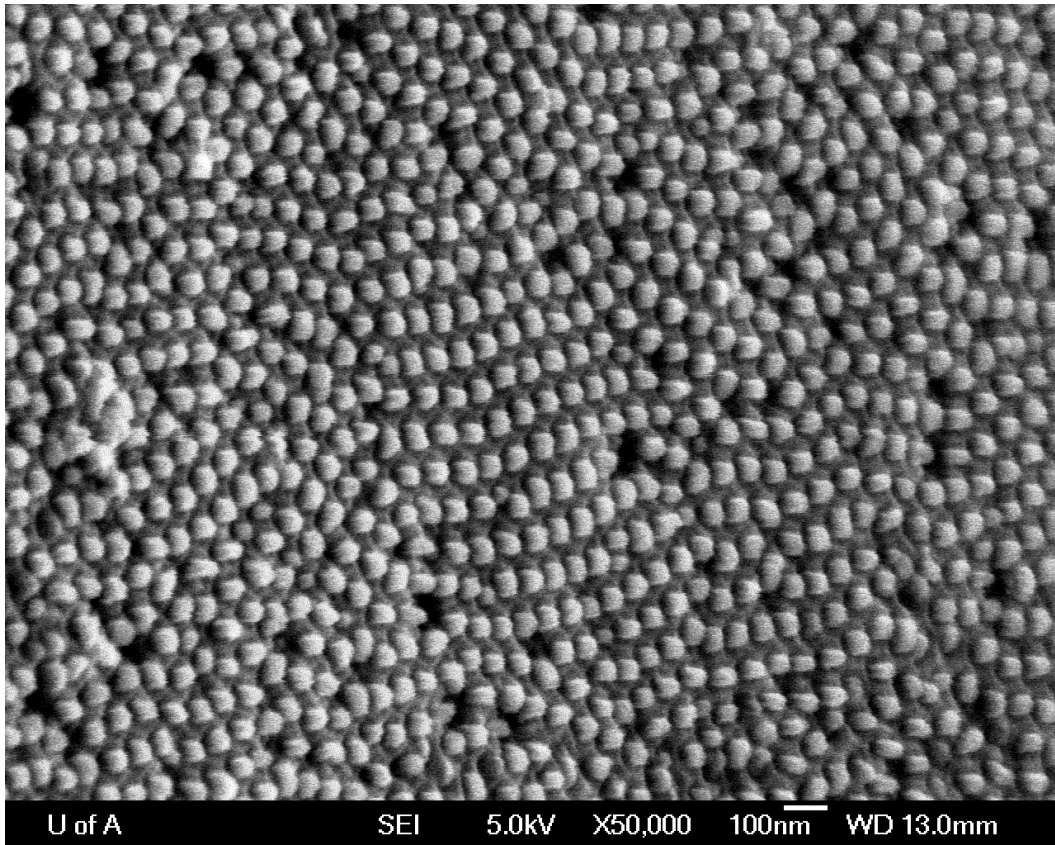


Figure 3.2 FESEM of the PCBM nanotube tips at the interface with bottom Co nanowires. It is evident the PCBM nanotubes are closed at the bottom.

Figure 3.2 shows the array of PCBM nanotubes (without cobalt) exposed from the backside of the template. The bottom tips of the PCBM nanotubes are closed, which is a characteristic of the organic growth process [1] mentioned in Chapter 2. The hollow nature of the tubes is evident from Figure 2.6. We estimate the outer shell diameter to be ~ 70 nm and inner shell diameter to be ~ 45 nm.

Figure 3.3 shows the cross-sectional image of the array based spin valve device. The tube length is ~ 325 nm. We also prepared another set of spin valve samples with slightly longer (~ 332 nm) PCBM nanotubes.

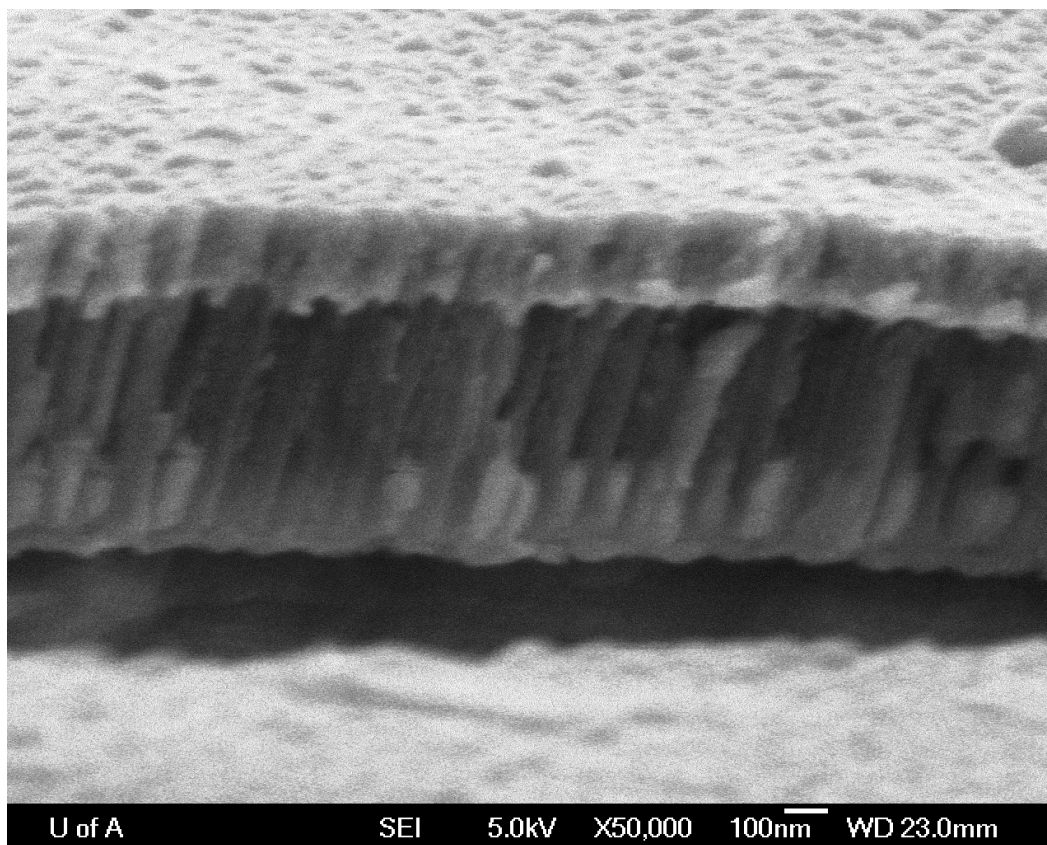


Figure 3.3 FESEM of cross section of final tri-layer (Co nanowire/PCBM nanotube/Ni thin film) device.

3.4 Device Characterization

As evidenced by the Figures 2.2, 2.4, 2.6 and 3.2 (empty and full templates), this centrifuge assisted method produces continuous nanotubes. The nanotubes, fabricated inside the pores of the AAO template, are vertically aligned, are uniform, are electrically isolated from one another and have capped bottoms. The outer diameter of the nanotubes is determined by the diameter of pores in the template. They can be successfully fabricated on several different substrates, which lead to the potential application of these structures in many devices outlined later.

3.4.1 Raman Characterization of PCBM Nanotubes

To further verify that the material inside the pores of Figure 2.6 is in fact PCBM, Raman spectroscopy of the filled templates has been performed. Studies are

limited on the Raman spectrum of PCBM thin films and not existent, to our knowledge, on PCBM nanowires and nanotubes. However, we can compare the Raman data from our experiments to the limited literature results available as well as that of fullerene (C_{60}) as the molecules are very similar in structure and show comparable vibrational modes from literature. We observe Raman peaks at 1430, 1463, and 1577 cm^{-1} (Figure 3.4), which correspond to the $T_{1u}(4)$, $A_g(2)$, and $H_g(8)$ modes, respectively. This matches well with literature values of 1429, 1470 and 1575 cm^{-1} for pristine C_{60} [109] and 1429, 1465 and 1573 cm^{-1} for pristine PCBM for the same respective modes [110]. This shows that there is no significant shift in the Raman peaks due to nanotube geometry and supports the fact that we do in fact have PCBM existent within nanopores.

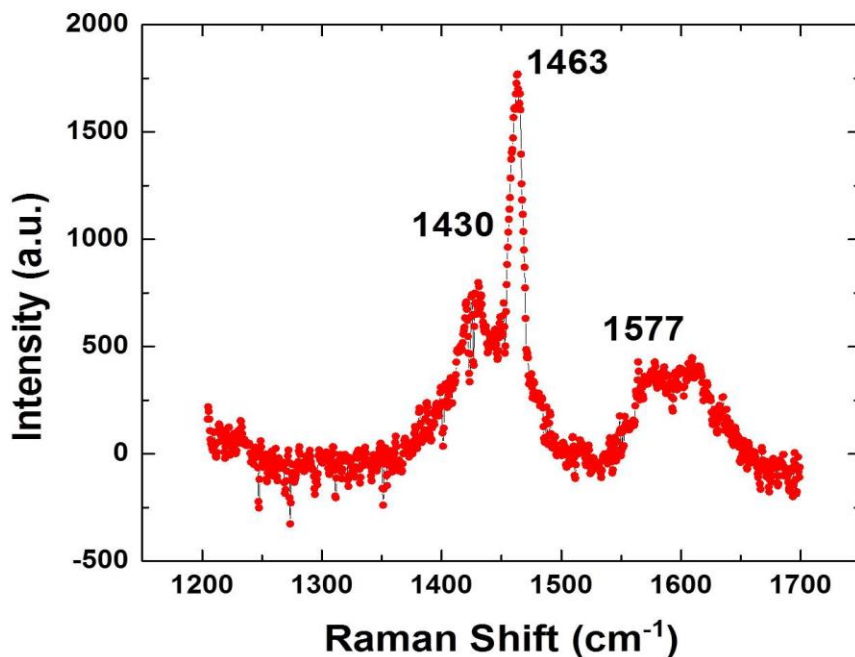


Figure 3.4 Raman spectrum of PCBM nanotubes imbedded in Al_2O_3 template.

3.4.2 XRD Characterization of PCBM Nanotubes

X-ray diffraction (XRD) has been performed on PCBM nanotubes, as shown in Figure 3.5. There are no apparent peaks in the XRD spectrum of nanotubes, suggesting lack of crystallinity. This is consistent with previous reports of XRD

analysis on spin-coated PCBM films [111]. The nanowire XRD data shown below has been taken following a mild annealing process performed at 140 °C for 4 min. [112]. Clearly, this annealing step is not sufficient to induce crystallinity.

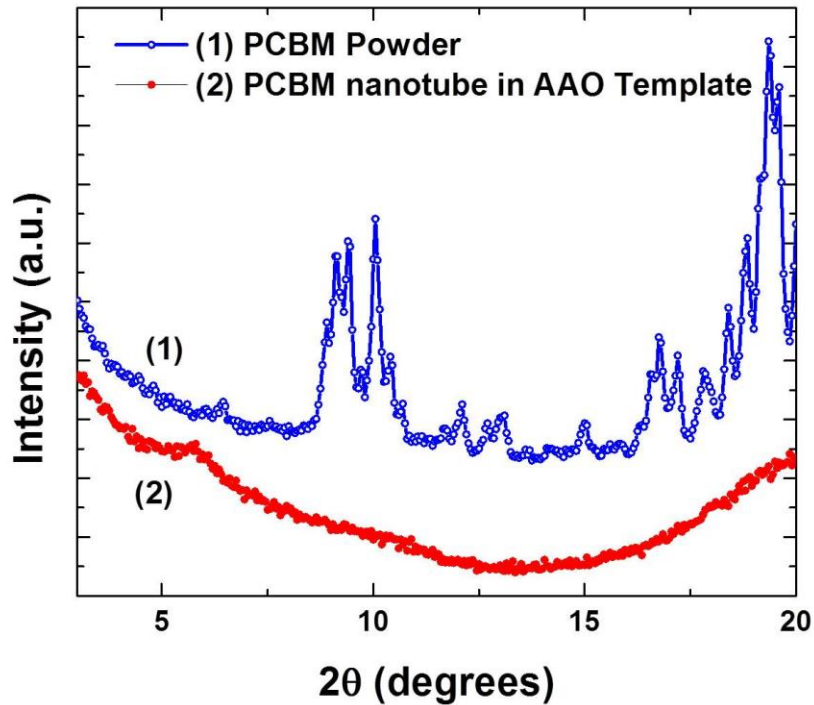


Figure 3.5 XRD spectrum of PCBM powder and PCBM nanotubes imbedded in the AAO matrix.

3.5 Charge Transport Measurements

Current-voltage (I-V) characteristics have been measured for ~ 30 nominally identical PCBM nanotube devices. Based on I-V characteristics, the samples can be classified into the following three representative categories: (a) linear (ohmic) behavior over the entire bias range (Figure 3.6a), (b) saturating I-V characteristics which is linear at low bias but gradually saturates as bias is increased (Figure 3.6b) and (c) non-linear I-V characteristics in which the current increases quadratically beyond a threshold voltage of ~ 2 – 3V (Figure 3.6c). Such a wide spread in I-V characteristic is quite common in metal/organic junctions and has

been reported before for other organics such as rubrene [113]. The origin of this spread lies in the variability of the nature of the metal-organic junctions (Schottky/ohmic/tunnel junctions) and the intrinsic variability in the organic growth process that significantly affects the molecular packing and the distribution of the trap states in the HOMO-LUMO gap [114].

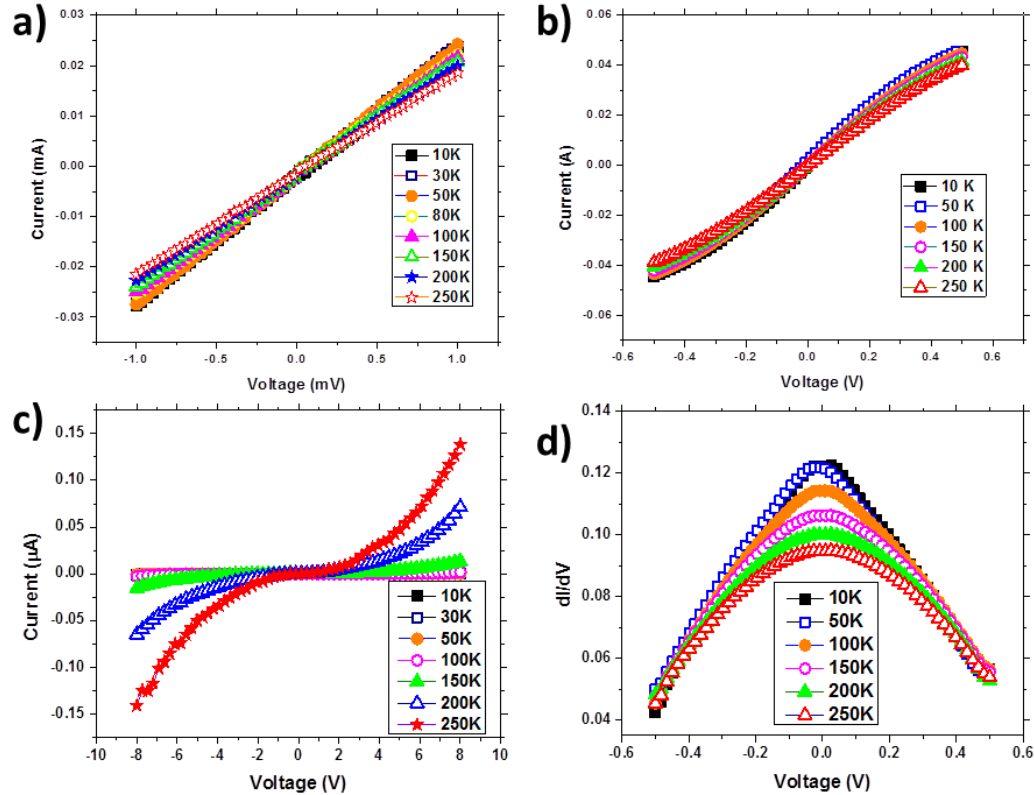


Figure 3.6 (a)-(c) Typical temperature-dependent current (I) vs. voltage (V) characteristics of ~ 325 nm long PCBM nanotubes embedded in alumina matrix. (d) Conductance (dI/dV) vs. voltage (V) characteristics for the devices in (b).

For the devices with linear I-V response (Figure 3.6a) the carriers do not appear to be localized – at least in the measured temperature and bias range. It is tempting to attribute this behavior to the resistance of the metallic contacts and/or pinhole shorts between the contacts. However, as shown later in this chapter, magnetoresistance of these samples is significantly different than the anisotropic magnetoresistance of the contacts. Additionally, the resistance of the contacts (measured on a control sample) is significantly smaller than the actual sample and

hence the observed I-V response cannot be simply attributed to the contact resistance.

Figure 3.6b shows the typical saturating I-V response. Such saturating behavior in both the positive and negative biases results in a pronounced positive “zero bias anomaly” in the differential conductance (Figure 3.6d). This type of response can be modeled (to the first order) as two back-to-back Schottky diodes (corresponding to Ni/PCBM and PCBM/Co junctions) connected in series [115]. With either direction of applied bias, one diode will be reverse biased and therefore limit the current allowed through the device. The current through such a device can be modeled as [115]:

$$I(V) = I_0 \tanh\left(\frac{eV}{2\eta kT}\right)$$

which can be derived from connecting two diodes in series (back-to-back) that have the following expression for their current [115]

$$I(V) = I_0 \left(e^{eV/\eta kT} - 1 \right)$$

Here η is the ideality factor for the Schottky diodes and can be determined graphically.

To determine the ideality factor, we have compared the theoretical differential conductance ($G(V) = dI/dV$) vs. bias (V) obtained from the above equation with the experimental data. By varying η we can see graphically which value of the ideality factor provides us with the closest match. This is done for all dI/dV curves at all temperatures as the ideality factor is temperature dependent. We note that the value of the ideality factor is very high, especially in the low temperature range (Figure 3.7a). This could be attributed to the fact that tunneling through the contact barrier is dominant at low temperatures. As described later, there are other sources of non-idealities that are not captured by the simple diode models mentioned above.

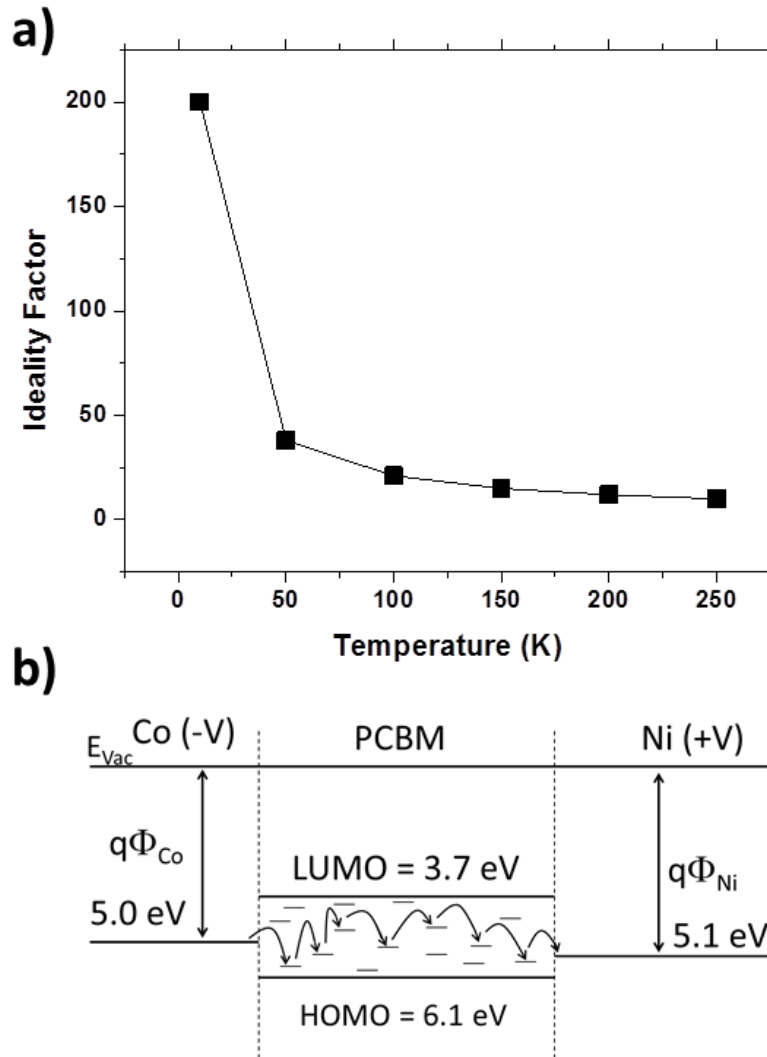


Figure 3.7 (a) Temperature dependence of ideality factor of diodes in spin-valve structure. (b) Rigid energy band diagram for the spin valve device and schematic description of the charge transport process.

Figure 3.6c shows the third type of I-V response, in which the current increases quadratically beyond a threshold voltage. No rectification effect has been observed. These devices exhibit a semiconducting behavior in the sense that resistivity decreases with increasing temperature. This effect can originate from various sources such as hopping conductance of PCBM nanotubes or thermionic injection of carriers at the contacts [114].

We note that in our devices the PCBM nanotubes are embedded in an alumina matrix, which is known to have a temperature-dependent trap state distribution [116]. We have shown before that the alumina matrix is amorphous in nature [1] and hosts trap states that can indirectly affect transport properties of the template-grown nanowires [20]. The alumina matrix has significant thermal expansion coefficient as noted by other studies [116] and hence its trap state distribution should strongly depend on temperature. Since the PCBM nanotubes are in close physical contact with alumina matrix, trap states in alumina can significantly affect the charge transport characteristics. These levels of complexity are however beyond the scope of the conventional charge transport models as described above [114].

The devices exhibiting the “saturating I-V characteristics” exhibit hysteresis effect in magnetoresistance measurements, as described below. Such hysteresis effects have not been observed for the samples exhibiting linear and non-linear I-V characteristics.

3.6 Magnetoresistance Measurements

Figure 3.8 shows the typical magnetoresistance traces of [Co nanowire/PCBM nanotube/Ni] spin valves at four different temperatures in the range of 25 – 290 K. In this work we represent magnetoresistance as $[R(B) - R(0)]/R(0)$, where R is the device resistance and B is the magnetic field in Gauss. In all measurements (including control experiments described later) B is parallel to the nanowire axis, which is also the direction of current. For the plots shown in Figure 3.8, no interfacial alumina barrier is present between the top Ni contact and the underlying PCBM nanotubes. A negative background magnetoresistance (i.e. decreasing device resistance with increasing strength of the external magnetic field) is present in all plots. We note that such background magnetoresistance is a common occurrence in organic spin valves [20], [25], [55], [56], [104], [105] and can have different origins [25]. Unlike Alq₃ nanowires reported before where a correlation between the signs of the spin valve signal and the background

magnetoresistance was observed [25], [55], for PCBM nanotubes we always find a negative background magnetoresistance and an associated inverse spin valve effect. Measurements performed on various control samples, presented later in this chapter, indicate that this background effect originates from the characteristic “organic magnetoresistance” of the PCBM layer [117] and cannot be attributed to anisotropic magnetoresistance of the contacts or fringe field effects. More importantly, in Figure 3.8 we observe a hysteretic negative peak in the device resistance between ~ 200 G and ~ 3000 G (at low temperatures), superimposed on the negative background magnetoresistance. Such negative peaks are the signatures of “inverse spin valve” effect, which is often observed in organic spin valves [55], [104], [105].

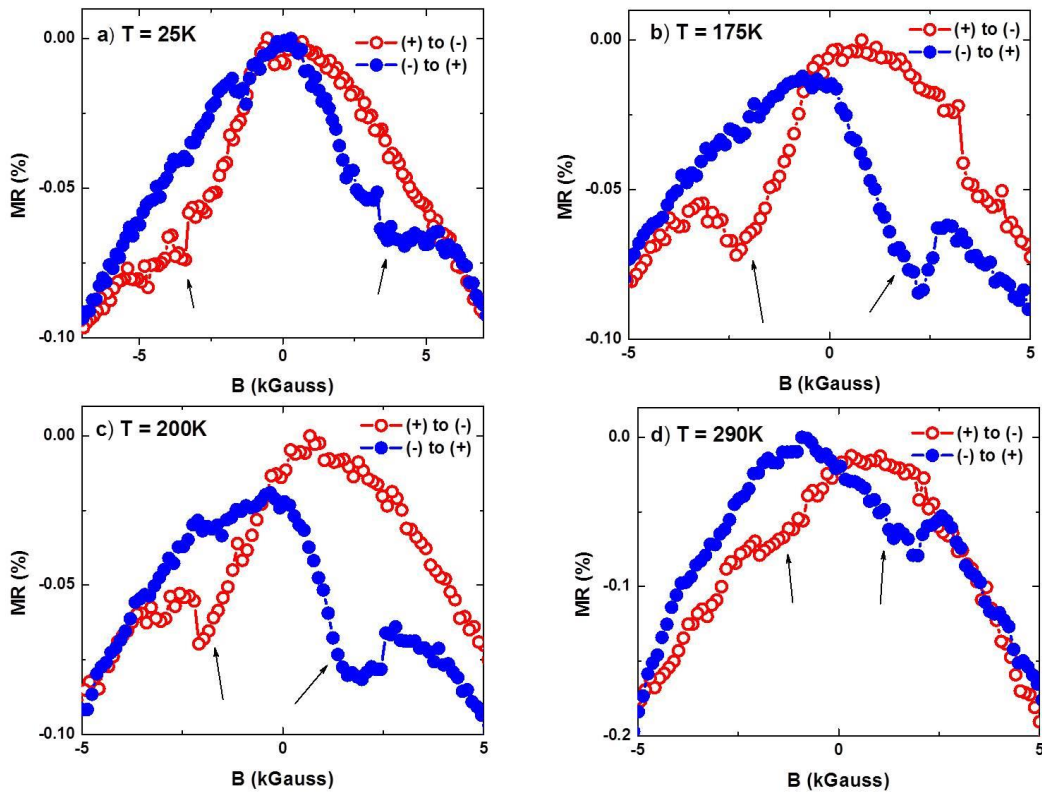


Figure 3.8 Magnetoresistance scans of [Co nanowire/PCBM nanotube/Ni] spin valves (without interfacial alumina barrier) for (a) 25K, (b) 175K, (c) 200K, and (d) 290K. MR is defined as $(R(B)-R_{max})/R_{max}$. The PCBM nanotube length is ~ 325 nm and magnetic field is parallel to the direction of current. The arrows indicate the (inverse) spin valve peaks.

The magnetization properties of the unassembled ferromagnetic contacts have been studied in detail in our previous work [56]. Typical low-temperature coercive fields are $\sim 180\text{G}$ and $\sim 1400\text{G}$ for Ni film and Co nanowires respectively [56]. The switching fields in the spin-valve devices are, in general, higher than the coercive field values of the unassembled ferromagnetic electrodes [56]. The reason for this offset is not clearly understood at this point, but we note that such mismatch has been recently observed by another group [118] in fullerene-based spin valves. In a spin valve device spin-dependent transmission depends on the magnetization properties of the interface, rather than the magnetization properties of the bulk. It is well known that magnetization properties of the metal-organic interface are strongly affected by the hybridization between the 3d states of the ferromagnets and the molecular orbitals of the organics [114], [119], [120] and can even cause inversion of the spin valve effect. Such effects are presumably responsible for the observed mismatch mentioned above.

To confirm that above-mentioned magnetoresistance responses do not originate from any other artifact, such as anisotropic magnetoresistance of the ferromagnetic contacts [121] or “local Hall effect” due to fringing fields of the ferromagnets [122], we have performed a series of control experiments described later in this chapter. The results obtained from these control experiments establish that the signals observed in Figure 3.8 can be attributed to spin dependent transport through the PCBM nanotubes. We note that the inverse spin valve effect persists even at room temperature (Figure 3.8d).

Figure 3.9 shows the magnetoresistance measurements on the PCBM nanotube spin valves in which an alumina barrier ($\sim 1\text{nm}$ thickness) exists at the interface between the top nickel contact and the underlying PCBM nanotubes. As described before, one of the major advantages of such interfacial tunnel barriers is that they prevent interdiffusion of metal species within the “soft” organics [105] in the vertical configuration. This interdiffusion often results in poor surface magnetization for the top contact and vanishing contact spin polarization below room temperature, even though Curie temperature of the ferromagnetic contacts

are much higher than room temperature [123]. As a result, spin valve signal disappears much below room temperature even though spin relaxation processes

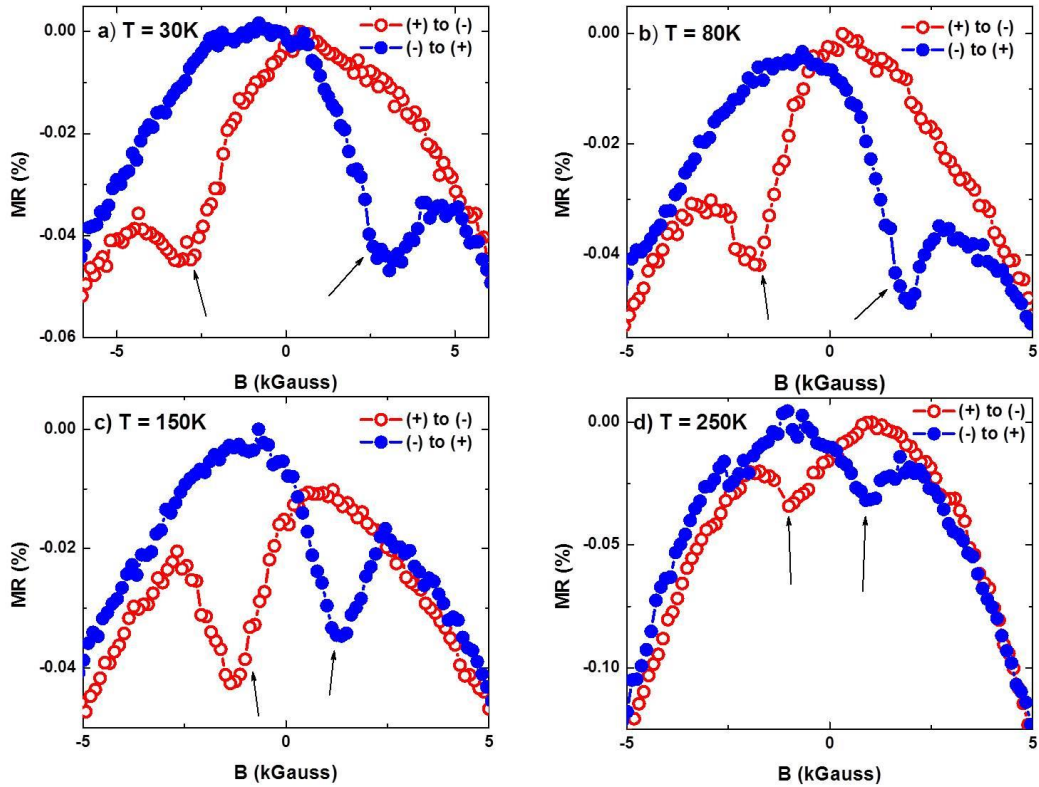


Figure 3.9 Magnetoresistance measurements of [Co nanowire/PCBM nanotube/alumina barrier/Ni] spin valves for (a) 30K, (b) 80K, (c) 150K, and (d) 250K. As before, the PCBM nanotubes are ~325 nm long, magnetic field is parallel to the direction of current, and MR is defined as $(R(B)-R_{max})/R_{max}$. The arrows indicate the (inverse) spin valve peaks.

in organics are weakly dependent on temperature [20]. However, for PCBM nanotubes, Figure 3.9 shows magnetoresistance behaviors that are very similar to those of Figure 3.8 and no significant improvement (except somewhat sharper switching) in the signal strength has been observed due to the presence of the alumina barrier. This is consistent with previous studies which noted that fullerene based molecules are more “robust” against interdiffusion compared to other organics (such as Alq₃) and hence direct deposition of the top ferromagnetic contact does not deteriorate the interface quality for fullerene-based systems [63],

[118]. As a result, spin-dependent transport and room temperature operation can be expected in fullerene-based organics even without an interfacial tunnel barrier.

Figure 3.10 shows the magnetoresistance plots of the spin valve devices in which no interfacial alumina barrier is present and the PCBM nanotubes are slightly longer (~ 332 nm) than before. In this case, the spin valve signal is significantly weaker compared to previous cases (Figures 3.8 and 3.9), though the background magnetoresistance persists. Such thickness dependence of the spin valve signal is consistent with the physical picture of spin dependent transport in the PCBM

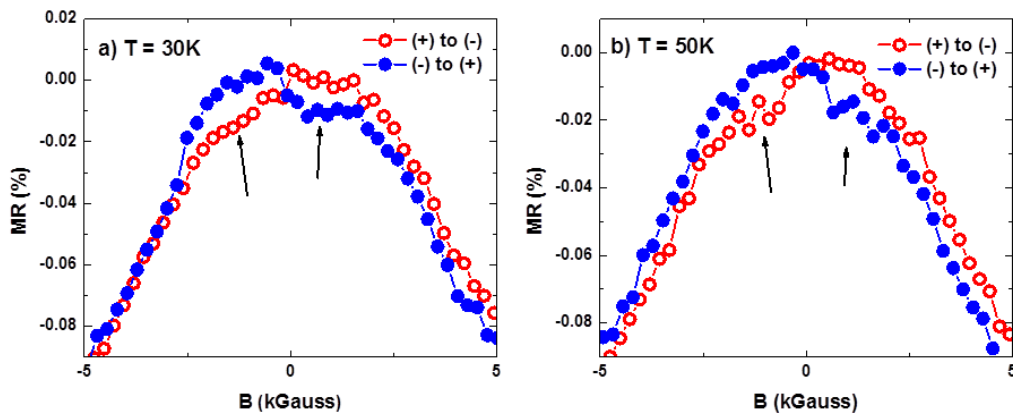


Figure 3.10 Magnetoresistance traces for the spin valve samples with longer average PCBM tube length of ~ 332 nm. As expected, the spin valve peaks are weaker than the previous cases (at similar temperatures) where the PCBM tube length was shorter (~ 325 nm). The arrows indicate the locations of the spin valve peaks.

segment since longer tube length will cause more spin depolarization before the spins are detected at the detector ferromagnet [20], [104]. As a result, longer tubes should result in weaker spin valve peaks, which we observe. A qualitative model that captures this feature is described below. We also note that in Figures 3.8-3.10, the switching fields of the contacts increase significantly with decreasing temperature. This is a characteristic of organic-based spin valves (in particular fullerene-based spin valves [118]) and is often attributed to pinning of domains on the organic surface [124].

The relative change in resistance ($\Delta R/R$) due to the spin valve peaks described before can be related to the device parameters by the so-called “modified Julliere formula” [20], [104]:

$$\frac{\Delta R}{R} = \frac{2P_1P_2e^{-d/L_s}}{1 - P_1P_2e^{-d/L_s}}$$

Here P_1 is the tunneling spin polarization of the injected carriers, which can be experimentally determined by the Meservey-Tedrow technique [125]. Once injected in the PCBM nanotubes, these carriers hop towards the second ferromagnetic contact (or “detector”), under the influence of the transport-driving electric field. The spin polarization of the injected carriers (P_1) decreases with distance x (measured from the injection point) and this spin relaxation process can be modeled as an exponential decay [20], [104], $P(x) = P_1 \exp(-x/L_s)$, where L_s is the spin relaxation length in the PCBM nanotubes. Exponential decay of spin polarization with distance has also been confirmed experimentally for other organics [103]. Thus when the carriers arrive at the detector interface, their spin polarization becomes $P(x) = P_1 \exp(-d/L_s)$, where d is the distance between the injector and the detector contacts i.e. the length of the PCBM nanotube. Now, application of the original Julliere formula [125] at the detector interface (assuming that the detector has a tunneling spin polarization of P_2) yields the “modified Julliere formula mentioned above. In literature this formula has been widely used to estimate L_s [18].

In almost all applications of this model, the quantities P_1, P_2 are taken directly from literature [125] and may not necessarily represent the exact values of tunneling spin polarization relevant for a particular experiment. For purely organic or organic-inorganic hybrid barriers, spin polarizations of the ferromagnets have been found to be less than the tabulated values [36]. Further, any surface imperfection can also reduce P_1 and P_2 . To include these effects, P_1 and P_2 can be replaced by $\alpha_1 P_1$ and $\alpha_2 P_2$ respectively, where $0 \leq \alpha_1, \alpha_2 \leq 1$. Since these “non-ideality factors” (α_1, α_2) are generally unknown, the estimated

L_S provides a lower bound of the actual spin relaxation length. We note that in a recent work [65], it has been pointed out that even in the absence of any spin relaxation, multistep tunneling can reduce the magnetoresistance. If this process is operative, the above-mentioned analysis based on modified Julliere formula, will yield even more conservative estimate of L_S .

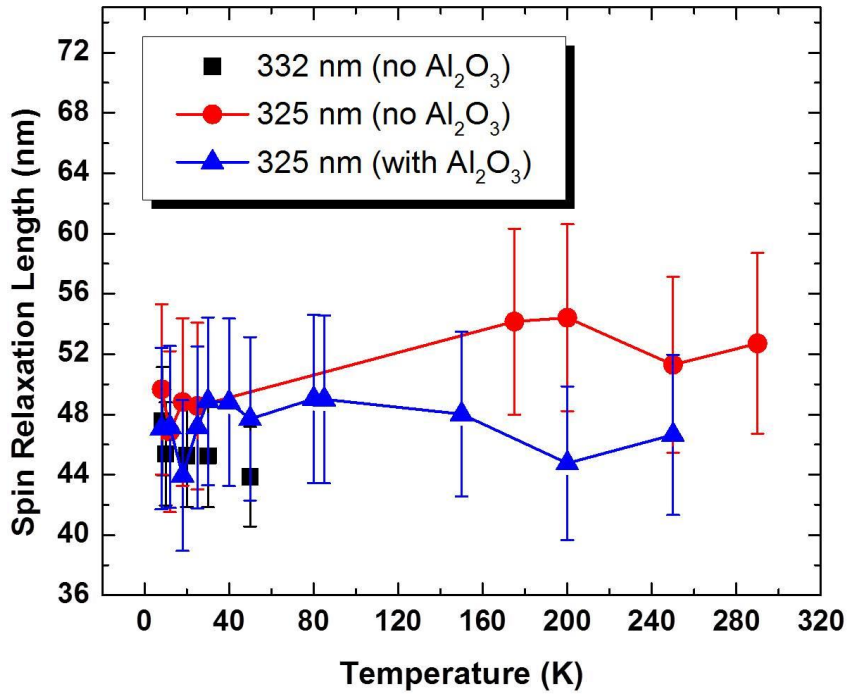


Figure 3.11 Spin relaxation length as a function of temperature for two sets of samples. Average length of PCBM nanotubes is ~ 325 nm in one set and ~ 332 nm in the other set. The error bars represent the variation in estimated spin relaxation length due to $\sim 10\%$ variation in the PCBM nanotube length.

Figure 3.11 shows the estimated spin relaxation length (lower bound) as a function of temperature T . We have assumed $P_1 = 33\%$ (Ni), $P_2 = 42\%$ (Co) [125] and $d = 325$ nm, as determined from the cross-sectional FESEM images. Spin relaxation length is relatively independent of temperature and a sizable estimate (~ 50 nm) is obtained *even at room temperature*. This is rather encouraging since these values, which are severely conservative estimates of $L_S(T)$, are obtained from devices with unoptimized transport properties. The

alumina barrier does not introduce any significant change in the $L_s - T$ characteristics. For samples with longer average PCBM tube length ($d \sim 332 \text{ nm}$), spin valve signal is weaker (Figure 3.10, as expected from the modified Julliere model described above), but the extracted L_s value matches well with the values determined from shorter tube length samples. This further indicates that the notches in the magnetoresistance plot indeed originate from the spin valve effect.

To investigate the role of any electrode-induced artifact such as anisotropic magnetoresistance effect [121] or local Hall effects induced by the ferromagnetic contacts which can potentially mimic spin valve signal [122], we have studied the following control samples: (i) [Co nanowire/Ni], (ii) [Co nanowire/PCBM nanotube/Ag], (iii) [Al/PCBM nanotube/Ni], and (iv) [Al/PCBM nanotube/Ag] control samples, while keeping the sample dimension same as the previous spin valve samples. Magnetoresistance of these control samples are presented later in this chapter. Spin valve signal is not present in any of these devices. This indicates that the spin valve peaks observed before (Figures 3.8-3.10) do not originate from anisotropic magnetoresistance effect or local Hall field due to the ferromagnetic contacts. Interestingly, all PCBM-containing devices exhibit a negative background magnetoresistance, which is very similar to that observed in Figures 3.8, 3.9 and 3.10. This effect therefore originates from the intrinsic “organic magnetoresistance” of PCBM, which has been observed before in thin film devices [117].

It is also possible to qualitatively understand why saturating IV characteristics (Figure 3.6b) is correlated with spin valve effect. As described before the saturating IV characteristics can be approximately modeled as two back-to-back Schottky barriers. Presence of interfacial Schottky barriers is known to facilitate spin selective transmission and circumvent the infamous conductivity mismatch problem [18]. Such barriers are not present in the linear IV samples (Figure 3.6a) and as a result we do not observe any spin valve effect. For the samples in Figure 3.6c, hopping conduction in PCBM nanotubes and/or thermionic injection of

carriers is dominant. Enhanced hopping increases spin relaxation and thermionic injection is not spin selective [18]. Thus no spin valve signal is observed in these samples.

3.7 Effect of Contacts on Magnetoresistance

To investigate the role of any electrode induced artifacts (such as the anisotropic magnetoresistance effect or local Hall effects induced by the ferromagnetic contacts), we have prepared (i) [Co nanowire/ Ni], (ii) [Co nanowire/PCBM nanotube/Ag], (iii) [Al/PCBM nanotube/Ni], (iv) [Al/PCBM nanotube/Ag] control samples, while keeping the sample dimensions same as the previous spin valve samples. Clearly, none of these samples exhibit any spin valve phenomenon as shown in Figure 3.12. For [Co nanowire/Ni] bilayer control samples (*without* the intermediate PCBM spacer), (a) the resistance is orders of magnitude smaller than the PCBM-containing devices (for a given contact area), and (b) [Co nanowire/Ni] samples exhibit *positive* anisotropic magnetoresistance (current parallel to the magnetic field configuration) as shown in Figure 3.12a, whereas all PCBM-containing samples exhibit a *negative* background magnetoresistance under the same condition. No sharp spin valve type switching is observed in [Co nanowire/Ni] samples, which is consistent with prior work [25], [121] that studied magnetoresistance of template-grown ferromagnetic nanowire arrays. Due to the reasons mentioned above, anisotropic magnetoresistance of the ferromagnetic contacts or pinhole short in the organic spacer cannot be used to explain the magnetoresistance behavior observed in Figures 3.8-3.10.

The PCBM-containing control samples (Figure 3.12, b-d) do not exhibit any spin valve signal but always show a negative background magnetoresistance, which was also observed in the spin valve samples (Figures 3.8-3.10). Thus we conclude that the spin valve peaks observed before do not originate from local Hall field artifacts due to the ferromagnetic contacts. The background magnetoresistance effect is present even when none of the contacts are ferromagnetic. This data therefore indicates that background magnetoresistance originates from the PCBM layer (i.e. organic magnetoresistance) and not from the

local Hall effects due to the ferromagnetic contacts. This feature is consistent with previous reports of organic magnetoresistance observed in PCBM thin films [117].

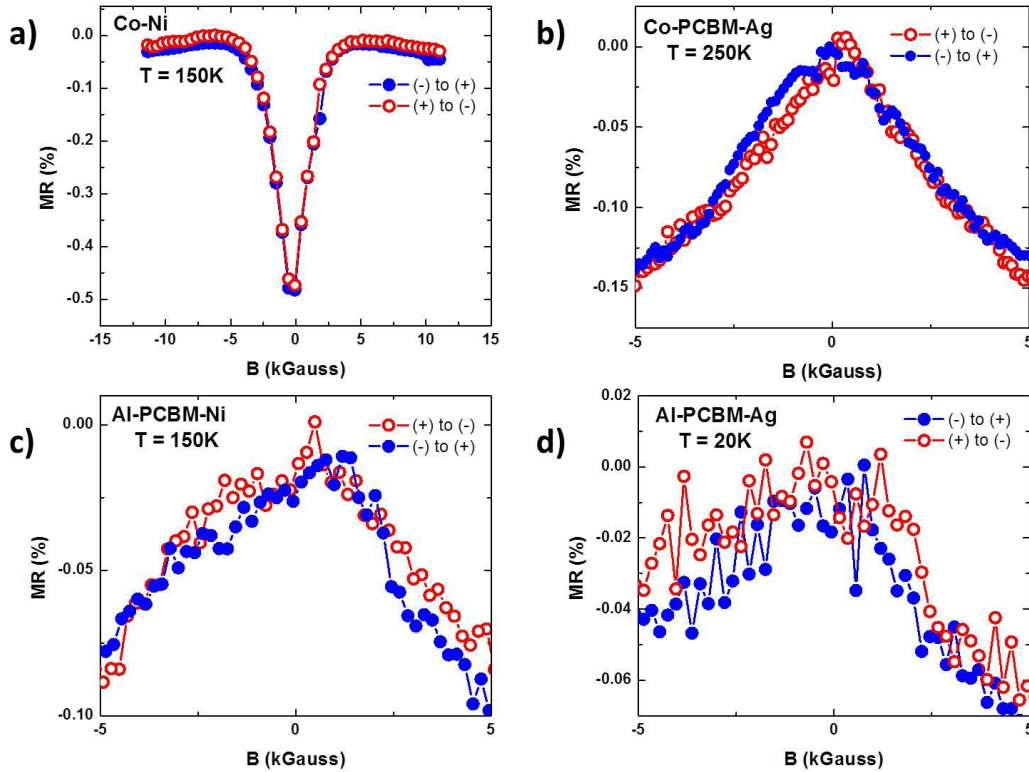


Figure 3.12 Effect of contacts on magnetoresistance. (a) Anisotropic magnetoresistance traces for the [Co nanowire/Ni] bilayered control samples, which have no PCBM layer. Typical positive magnetoresistance effect is observed, which occurs when magnetic field is parallel to the direction of current. (b), (c) Magnetoresistance measurements on trilayered samples with only one ferromagnetic contact. No spin-valve peaks have been observed, but the negative background magnetoresistance is present. (d) Magnetoresistance measurements on trilayered samples with no ferromagnetic contact. The background magnetoresistance is still present in this sample.

3.8 Magnetoresistance of [Ni film – PCBM nanotube – Co nanowire] Samples Exhibiting Linear I-V Characteristics:

As described earlier in this chapter, PCBM spin valve samples that exhibit linear *I-V* characteristics do not exhibit any spin valve effect. However, these samples show a negative background magnetoresistance as shown in Figure 3.13.

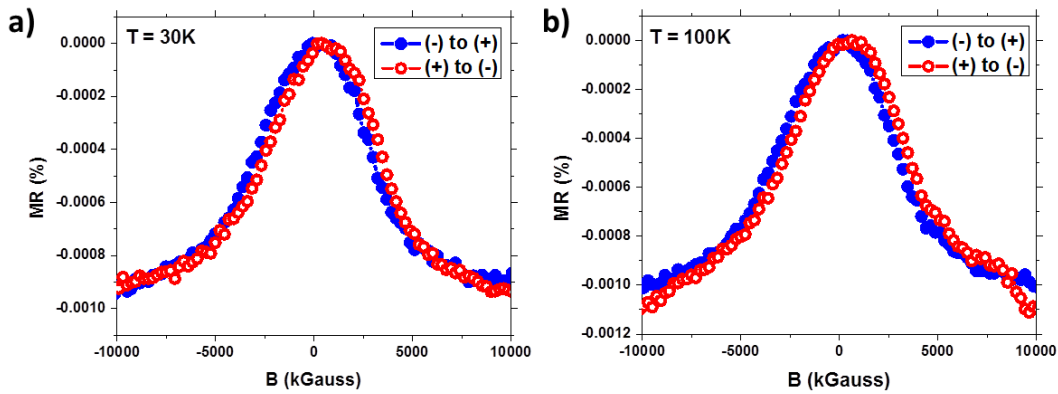


Figure 3.13 Absence of spin valve effect in Ni-PCBM-Co devices that exhibit linear I-V response.

3.9 Conclusion

In conclusion, we have shown spin-polarized transport in vertical array of PCBM nanotubes. This phenomenon persists even at room temperature and makes this system promising for development of room temperature nanotube-based spintronic devices and circuits. For example, vertically standing PCBM nanotube spin valves can be synthesized on a bottom aluminum electrode patterned in the form of an array of nanoscale bars. On the top surface another set of parallel bars can be formed which run perpendicular to the bottom electrode array. Thus the nanotube spin valves will be connected at the cross points of a nanoscale crossbar architecture [126], which is a rudimentary nanospintronic memory circuit. Signal strength can be further improved by shortening the length of the nanotubes, by controlling the fabrication parameters (further details are in Chapter 4). The host alumina matrix indirectly affects the charge (and hence spin) transport process. Thermal annealing [116], post-growth selective removal of alumina followed by conformal deposition of high quality dielectric [116], [127], can offer further improvement in device performance. The reported PCBM nanotube spin valves do not require an interfacial tunnel barrier to operate, which significantly simplifies the device fabrication process.

Chapter 4. Future/Ongoing Work

We have obtained very encouraging results from our measurements to date. However, we know that with some more work and some slight adjustments to the device fabrication process and design, we can improve upon the signal strength we currently observe. Here we will present some of the modifications that can lead to a much improved device as well as the progress of parallel projects.

4.1 Improving Spin-Valve Response

While the spin-valve signal from these PCBM nanotube devices persists at room temperature, there is still work needed to be done to improve the signal to a level that can be implemented in practical devices. There are several properties and characteristics of the spin-valve device that can be modified to improve the spin-valve signal.

The first, and most obvious, way to improve the spin-valve signal of this device, and similar nanowire geometry devices, is to reduce the length of the organic (PCBM) nanowire. We can see this is the case by analyzing the modified Julliere formula in Chapter 3. L_s is a property inherent to the device structure and its materials, which cannot be easily manipulated without changing those materials. d is a much easier parameter to change as it only represents the PCBM nanotube length. The centrifuge-assisted organic nanowire deposition method cannot vary the length of the nanowire on its own, but there are two other ways we can modify steps already in the fabrication procedure to produce shorter organic nanowires. We can 1) reduce the time of the final anodization step to give a thinner starting template and shorter pores or, 2) increase the time of electrodeposition for the cobalt nanowires, which will increase their length filling up a larger percentage of the empty pore. Both of these approaches will leave a smaller amount of empty pore at the top of the template resulting in a shorter organic nanowire. This is due to the inherent characteristic of filling all remaining empty pore space associated with the centrifuge deposition method. As electrons are injected in to one end of the nanowire they possess some polarization of electron spin, described by P_1 and

P_2 , which begins to decay or “relax” back to a net zero polarization over time and distance (d) travelled in the nanowire. For this reason, the shorter the length of organic nanowire we can fabricate, the stronger the spin current will be at the detector junction resulting in a larger spin valve signal. There is one more way to reduce the length of the organic nanowire, which is to introduce another step in the procedure that will subtract some of its length once it has been grown. One technique available to reduce the thickness of the entire device structure would be to use an ion mill. In ion milling, inert ions (typically Ar^+) are accelerated towards the surface of the template using an electric field. The ions bombard the surface of the template and etch it by essentially breaking off chunks of material from the surface. This will shave down the overall thickness of the template and more importantly the thickness of the organic nanotubes, again reducing d and improving the spin valve signal.

Another device feature that can introduce a large amount of spin relaxation is the metal-organic junction. There are two interfaces between a metal and the organic nanowire in a spin valve device, which for this device are the cobalt/PCBM and the PCBM/nickel junctions. As mentioned earlier, there are ways of improving the quality of given metal/organic junctions, such as introducing extremely thin interfacial barriers (i.e. alumina). These barrier layers serve multiple purposes such as preventing the interdiffusion of evaporated thin film contacts in to the soft organic material and mitigating the conductance mismatch issue of two adjacent materials. While it was shown in our magnetoresistance measurements that the inclusion of an alumina thin film barrier between the PCBM/nickel interface did not drastically improve the strength of the spin valve signal, it still remains a possible solution as it has worked well for other devices [36], [103], [108]. Because the cobalt nanowires are buried ~ 300 nm below the pore opening, it is extremely difficult to fabricate a similar interfacial barrier at the cobalt/PCBM junction. However, because the cobalt nanowire is fabricated prior to any organic material processing, it is already a solid material that will not interdiffuse in to the PCBM nanowire. Furthermore, annealing of the device prior to PCBM deposition can improve crystallinity of the cobalt nanowire, help to produce a well-defined

contact and introduce a thin cobalt oxide layer if done in atmosphere, which can help with conductance mismatch as the deposited alumina layer does for the opposite junction.

4.2 Hybrid Metamaterials⁴

Optoelectronics is a field that has shown lots of interest in metallic and semiconducting nanowires. By modifying the feature sizes of the nanowires, we can influence how these nanowires interact with light. The dimensions attainable by fabricating these nanowires in a transparent AAO matrix can allow them to exhibit plasmon resonance phenomenon. Plasmon resonance in short is the absorption of a specific band of light by the electrons in a material causing them to resonate at a characteristic frequency. This resonance is known as a plasmon. Many metallic and semiconducting nanowire materials have been studied but none, to our knowledge, have incorporated a hybrid design that combines characteristics of both metallic and semiconducting behaviors by fabricating axially heterostructured metal/organic nanowires. Currently we are exploring this intriguing design to uncover its potential applications as a light emitter and absorber. Fabrication of metallic, organic, and metal-organic hybrid nanowire arrays on glass substrates will be completed by me while spectroscopy techniques, measuring the performance of the devices will be done by collaborators under the supervision of Dr. Zubin Jacob.

To fabricate such devices, one key device requirement that differs from our spin-valve design is that the samples must be transparent. While the AAO matrix does satisfy this requirement for the visible range of the light spectrum, the presence of the aluminum foil substrate does not. To solve this problem, as also described in detail in Chapter 2, a thin film multilayer system is deposited on to a glass substrate to provide mechanical strength to the device while allowing light to pass through easily, interacting only with the nanowire imbedded AAO matrix.

⁴ A joint patent application has been filed for the structure and fabrication method of this device. Portions of this chapter have been taken from this application.

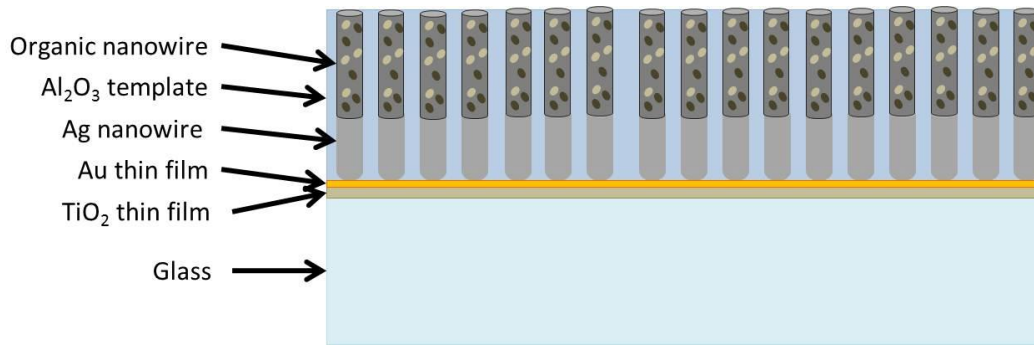


Figure 4.1 Schematic of proposed structure of metal-organic hybrid nanowire metamaterial device.

First, fabrication and modelling of electrodeposited silver nanowires imbedded in the AAO matrix will be completed. Comparisons will be made with literature to verify the plasmonic resonances of our samples appear at the proper wavelengths. The next step will be to incorporate our centrifuge-assisted organic nanowire fabrication to build our hybrid nanowire design. This organic nano-antenna architecture will increase the efficiency of organic light emitting diodes (OLED's) by allowing us to control and enhance the outcoupling efficiency, permitting improved light generation. With respect to organic photovoltaics (OPV's), our structure will create a larger scattering cross section while the presence of the nano-antennas is expected to increase light absorption compared to traditional thin film devices. Furthermore, the design is expected to show broadband absorption of the visible spectrum, something conventional photovoltaics have been struggling to achieve.

4.3 Coaxial Organic Nanowires for Radially Heterojunctioned Photovoltaic Devices

The state of the art device architecture for organic solar cells today is known as “bulk-heterojunction (BHJ)” architecture [128]. BHJ cells use a mixture of electron donor-acceptor materials (typically P3HT and PCBM) as the active layer in the cell structure. This layer is responsible for exciton generation and harvesting. While this blended layer of organic material is a huge improvement over single layer and bilayer geometries [129] as it greatly increases the donor-acceptor interface area, it is far from ideal. BHJ cells contain several flaws that

impede them from generating current such as (a) poor charge collection due to interfacial recombination of charge carriers, (b) formation of domain islands that trap charge carriers and provide no direct path to electrodes and (c) lack of specific structure, which introduces variability among devices. For efficient generation of photocurrent in organic materials we need the maximum distance between an exciton generation site and a heterojunction to be comparable to the exciton diffusion length (~10-20 nm). Also, the active layer needs to have a thickness comparable to the photon absorption length which is ~200-400 nm in organic materials.

We propose a structure similar to that of the metamaterials device in section 4.2. Here, we use the same AAO template on glass substrate to fabricate our devices. First we will grow a short metallic nanowire (Ag) in the bottom of the pore which will help create contact with the coaxial organic nanowire layer. Next we will deposit an acceptor material (PCBM) nanotube as we have done before making use of the centrifuge assisted deposition technique. This will serve as the shell of the nanowire and will create a good contact with the metallic nanowire due to its capped bottom. The hollow core of the nanotube will then be filled with a complementary donor material (P3HT) using the same centrifuge deposition technique. To avoid intermixing of the interfaces, a non-solvent for the shell material will be used as a solvent for the core material. Finally a top contact (ITO or aluminum) will be sputtered on the surface to serve as the second electrode of the device.

With a shell thickness of ~7-17 nm and pore diameters for AAO templates ranging from 20-50 nm, the core organic diameter is expected to be ~30 nm. With these active material lengths, exciton generation should almost always occur within one diffusion length of a heterojunction, potentially producing extremely high conversion efficiencies. Nanowire lengths can also be designed to exceed 400 nm, allowing them to comply with the photon absorption length of most organic semiconductors.

References

- [1] K. M. Alam, A. P. Singh, R. Starko-Bowes, S. C. Bodepudi, and S. Pramanik, "Template-Assisted Synthesis of π -Conjugated Molecular Organic Nanowires in the Sub-100 nm Regime and Device Implications," *Adv. Funct. Mater.*, vol. 22, no. 15, pp. 3298–3306, 2012.
- [2] C. K. Chiang, M. A. Druy, S. C. Gau, A. J. Heeger, E. J. Louis, A. G. MacDiarmid, Y. W. Park, and H. Shirakawa, "Synthesis of highly conducting films of derivatives of polyacetylene, (CH)_x," *J. Am. Chem. Soc.*, vol. 100, no. 3, pp. 1013–1015, Feb. 1978.
- [3] X. Zhao and X. Zhan, "Electron transporting semiconducting polymers in organic electronics," *Chem. Soc. Rev.*, vol. 40, no. 7, pp. 3728–3743, Jun. 2011.
- [4] N. Tessler, Y. Preezant, N. Rappaport, and Y. Roichman, "Charge Transport in Disordered Organic Materials and Its Relevance to Thin-Film Devices: A Tutorial Review," *Adv. Mater.*, vol. 21, no. 27, pp. 2741–2761, 2009.
- [5] C. Zhang, Y. Yan, Y. S. Zhao, and J. Yao, "Synthesis and applications of organic nanorods, nanowires and nanotubes," *Annu. Reports Sect. C Phys. Chem.*, Apr. 2013.
- [6] F. S. Kim, G. Ren, and S. A. Jenekhe, "One-Dimensional Nanostructures of π -Conjugated Molecular Systems: Assembly, Properties, and Applications from Photovoltaics, Sensors, and Nanophotonics to Nanoelectronics," *Chem. Mater.*, vol. 23, no. 3, pp. 682–732, Feb. 2011.
- [7] J. Hu, T. W. Odom, and C. M. Lieber, "Chemistry and Physics in One Dimension: Synthesis and Properties of Nanowires and Nanotubes," *Accounts Chem. Res.*, vol. 32, no. 5, pp. 435–445, May 1999.
- [8] W. C. W. Chan and S. Nie, "Quantum Dot Bioconjugates for Ultrasensitive Nonisotopic Detection," *Science*, vol. 281, no. 5385, pp. 2016–2018, Sep. 1998.
- [9] G. Chidichimo and L. Filippelli, "Organic Solar Cells: Problems and Perspectives," *Int. J. Photoenergy*, vol. 2010, Jul. 2010.
- [10] S. Günes, H. Neugebauer, and N. S. Sariciftci, "Conjugated Polymer-Based Organic Solar Cells," *Chem. Rev.*, vol. 107, no. 4, pp. 1324–1338, Apr. 2007.
- [11] J. E. Slota, X. He, and W. T. S. Huck, "Controlling nanoscale morphology in polymer photovoltaic devices," *Nano Today*, vol. 5, no. 3, pp. 231–242, Jun. 2010.
- [12] M. D. Kelzenberg, D. B. Turner-Evans, M. C. Putnam, S. W. Boettcher, R. M. Briggs, J. Y. Baek, N. S. Lewis, and H. A. Atwater, "High-performance Si microwire photovoltaics," *Energy Environ. Sci.*, vol. 4, no. 3, pp. 866–871, Mar. 2011.
- [13] M. Aryal, F. Buyukserin, K. Mielczarek, X.-M. Zhao, J. Gao, A. Zakhidov, and W. (Walter) Hu, "Imprinted large-scale high density polymer nanopillars for organic solar cells," 2008, vol. 26, pp. 2562–2566.
- [14] N. Haberkorn, J. S. Gutmann, and P. Theato, "Template-Assisted Fabrication of Free-Standing Nanorod Arrays of a Hole-Conducting Cross-Linked Triphenylamine Derivative: Toward Ordered Bulk-Heterojunction Solar Cells," *ACS Nano*, vol. 3, no. 6, pp. 1415–1422, Jun. 2009.
- [15] J. L. Duvail, Y. Long, S. Cuenot, Z. Chen, and C. Gu, "Tuning electrical properties of conjugated polymer nanowires with the diameter," *Appl. Phys. Lett.*, vol. 90, no. 10, pp. 102114–102114–3, Mar. 2007.
- [16] A. L. Briseno, S. C. B. Mannsfeld, S. A. Jenekhe, Z. Bao, and Y. Xia, "Introducing organic nanowire transistors," *Mater. Today*, vol. 11, no. 4, pp. 38–47, Apr. 2008.

- [17] V. A. Dediu, L. E. Hueso, I. Bergenti, and C. Taliani, "Spin routes in organic semiconductors," *Nat. Mater.*, vol. 8, no. 9, pp. 707–716, Aug. 2009.
- [18] K. M. Alam and S. Pramanik, "Spin Transport in Organic Semiconductors: A Brief Overview of the First Eight Years," in *Nano-Semiconductors*, CRC Press, 2011, pp. 87–133.
- [19] W. J. M. Naber, S. Faez, and W. G. van der Wiel, "Organic Spintronics," arXiv e-print cond-mat/0703455, Mar. 2007.
- [20] S. Pramanik, C.-G. Stefanita, S. Patibandla, S. Bandyopadhyay, K. Garre, N. Harth, and M. Cahay, "Observation of extremely long spin relaxation times in an organic nanowire spin valve," *Nat. Nanotechnol.*, vol. 2, no. 4, pp. 216–219, Apr. 2007.
- [21] B. Kanchibotla, S. Pramanik, S. Bandyopadhyay, and M. Cahay, "Transverse spin relaxation time in organic molecules," *Phys. Rev. B*, vol. 78, no. 19, p. 193306, Nov. 2008.
- [22] T. D. Nguyen, G. Hukic-Markosian, F. Wang, L. Wojcik, X.-G. Li, E. Ehrenfreund, and Z. V. Vardeny, "Isotope effect in spin response of [pi]-conjugated polymer films and devices," *Nat. Mater.*, vol. 9, no. 4, pp. 345–352, Feb. 2010.
- [23] Z. G. Yu, "Spin-Orbit Coupling, Spin Relaxation, and Spin Diffusion in Organic Solids," *Phys. Rev. Lett.*, vol. 106, no. 10, p. 106602, Mar. 2011.
- [24] L. Das, J. Mateo, S. Bandyopadhyay, S. Bandyopadhyay, J. D. Edwards, and J. Anderson, "Motional modes in bulk powder and few-molecule clusters of tris(8-hydroxyquinoline aluminum) and their relation to spin dephasing," *Appl. Phys. Lett.*, vol. 98, no. 6, pp. 063109–063109–3, Feb. 2011.
- [25] K. M. Alam and S. Pramanik, "High-field magnetoresistance in nanowire organic spin valves," *Phys. Rev. B*, vol. 83, no. 24, p. 245206, Jun. 2011.
- [26] D. H. Reneker and I. Chun, "Nanometre diameter fibres of polymer, produced by electrospinning," *Nanotechnology*, vol. 7, no. 3, p. 216, Sep. 1996.
- [27] D. H. Reneker, A. L. Yarin, H. Fong, and S. Koombhongse, "Bending instability of electrically charged liquid jets of polymer solutions in electrospinning," *J. Appl. Phys.*, vol. 87, no. 9, pp. 4531–4547, May 2000.
- [28] R. Kessick, J. Fenn, and G. Tepper, "The use of AC potentials in electrospinning and electrospinning processes," *Polymer*, vol. 45, no. 9, pp. 2981–2984, Apr. 2004.
- [29] B. Dong, D. Y. Zhong, L. F. Chi, and H. Fuchs, "Patterning of Conducting Polymers Based on a Random Copolymer Strategy: Toward the Facile Fabrication of Nanosensors Exclusively Based on Polymers," *Adv. Mater.*, vol. 17, no. 22, pp. 2736–2741, 2005.
- [30] Y. Chen and Y. Luo, "Precisely Defined Heterogeneous Conducting Polymer Nanowire Arrays – Fabrication and Chemical Sensing Applications," *Adv. Mater.*, vol. 21, no. 20, pp. 2040–2044, 2009.
- [31] J. G. Park, G. T. Kim, J. H. Park, H. Y. Yu, G. McIntosh, V. Krstic, S. H. Jhang, B. Kim, S. H. Lee, S. W. Lee, M. Burghard, S. Roth, and Y. W. Park, "Quantum transport in low-dimensional organic nanostructures," *Thin Solid Films*, vol. 393, no. 1–2, pp. 161–167, Aug. 2001.
- [32] O. Fenwick, L. Bozec, D. Credgington, A. Hammiche, G. M. Lazzerini, Y. R. Silberberg, and F. Cacialli, "Thermochemical nanopatterning of organic semiconductors," *Nat. Nanotechnol.*, vol. 4, no. 10, pp. 664–668, Oct. 2009.
- [33] S.-Y. Jang, M. Marquez, and G. A. Sotzing, "Rapid Direct Nanowriting of Conductive Polymer via Electrochemical Oxidative Nanolithography," *J. Am. Chem. Soc.*, vol. 126, no. 31, pp. 9476–9477, Aug. 2004.

- [34] Y. Xia and G. M. Whitesides, "Soft Lithography," *Angew. Chem. Int. Ed.*, vol. 37, no. 5, pp. 550–575, 1998.
- [35] B. D. Gates, Q. Xu, J. C. Love, D. B. Wolfe, and G. M. Whitesides, "Unconventional Nanofabrication," *Annu. Rev. Mater. Res.*, vol. 34, no. 1, pp. 339–372, 2004.
- [36] T. S. Santos, J. S. Lee, P. Migdal, I. C. Lekshmi, B. Satpati, and J. S. Moodera, "Room-Temperature Tunnel Magnetoresistance and Spin-Polarized Tunneling through an Organic Semiconductor Barrier," *Phys. Rev. Lett.*, vol. 98, no. 1, p. 016601, Jan. 2007.
- [37] Y. Q. Zhan, I. Bergenti, L. E. Hueso, V. Dediu, M. P. de Jong, and Z. S. Li, "Alignment of energy levels at the $\text{Alq}_3/\text{La}_{0.7}\text{Sr}_{0.3}\text{MnO}_3$ interface for organic spintronic devices," *Phys. Rev. B*, vol. 76, no. 4, p. 045406, Jul. 2007.
- [38] G. M. Whitesides, J. P. Mathias, and C. T. Seto, "Molecular self-assembly and nanochemistry: a chemical strategy for the synthesis of nanostructures," *Science*, vol. 254, no. 5036, pp. 1312–1319, Nov. 1991.
- [39] G. M. Whitesides and B. Grzybowski, "Self-Assembly at All Scales," *Science*, vol. 295, no. 5564, pp. 2418–2421, Mar. 2002.
- [40] F. J. M. Hoeben, P. Jonkheijm, E. W. Meijer, and A. P. H. J. Schenning, "About Supramolecular Assemblies of π -Conjugated Systems," *Chem. Rev.*, vol. 105, no. 4, pp. 1491–1546, Apr. 2005.
- [41] A. P. H. J. Schenning and E. W. Meijer, "Supramolecular electronics; nanowires from self-assembled π -conjugated systems," *Chem. Commun.*, no. 26, pp. 3245–3258, Jun. 2005.
- [42] D. H. Kim, D. Y. Lee, H. S. Lee, W. H. Lee, Y. H. Kim, J. I. Han, and K. Cho, "High-Mobility Organic Transistors Based on Single-Crystalline Microribbons of Triisopropylsilylethynyl Pentacene via Solution-Phase Self-Assembly," *Adv. Mater.*, vol. 19, no. 5, pp. 678–682, 2007.
- [43] A. L. Briseno, S. C. B. Mannsfeld, X. Lu, Y. Xiong, S. A. Jenekhe, Z. Bao, and Y. Xia, "Fabrication of Field-Effect Transistors from Hexathiapentacene Single-Crystal Nanowires," *Nano Lett.*, vol. 7, no. 3, pp. 668–675, Mar. 2007.
- [44] J. Jang, B. Lim, J. Lee, and T. Hyeon, "Fabrication of a novel polypyrrole/poly(methyl methacrylate) coaxial nanocable using mesoporous silica as a nanoreactor," *Chem. Commun.*, no. 1, pp. 83–84, Jan. 2001.
- [45] C.-G. Wu and T. Bein, "Polyaniline Wires in Oxidant-Containing Mesoporous Channel Hosts," *Chem. Mater.*, vol. 6, no. 8, pp. 1109–1112, Aug. 1994.
- [46] L. Dauginet-De Pra, E. Ferain, R. Legras, and S. Demoustier-Champagne, "Fabrication of a new generation of track-etched templates and their use for the synthesis of metallic and organic nanostructures," *Nucl. Instruments Methods Phys. Res. Sect. B Beam Interactions Mater. Atoms*, vol. 196, no. 1–2, pp. 81–88, Nov. 2002.
- [47] F. Nasirpouri, P. Southern, M. Ghorbani, A. Irajizad, and W. Schwarzacher, "GMR in multilayered nanowires electrodeposited in track-etched polyester and polycarbonate membranes," *J. Magn. Magn. Mater.*, vol. 308, no. 1, pp. 35–39, Jan. 2007.
- [48] R. Starke-Bowes and S. Pramanik, "Ultrahigh Density Array of Vertically Aligned Small-molecular Organic Nanowires on Arbitrary Substrates," *J. Vis. Exp.*, no. 76, Jun. 2013.
- [49] T. D. Brock, *Membrane filtration: a user's guide and reference manual*. Science Tech, 1983.

- [50] M. Delvaux, J. Duchet, P.-Y. Stavaux, R. Legras, and S. Demoustier-Champagne, “Chemical and electrochemical synthesis of polyaniline micro- and nano-tubules,” *Synth. Met.*, vol. 113, no. 3, pp. 275–280, Jun. 2000.
- [51] B. Heinrich and J. A. C. Bland, *Ultrathin Magnetic Structures IV: Applications of Nanomagnetism (Chapter 7)*. Springer, 2005.
- [52] M. Gobbi, A. Pascual, F. Golmar, R. Llopis, P. Vavassori, F. Casanova, and L. E. Hueso, “C60/NiFe combination as a promising platform for molecular spintronics,” *Org. Electron.*, vol. 13, no. 3, pp. 366–372, Mar. 2012.
- [53] S. K. Biswas, R. Vajtai, B. Wei, G. Meng, L. J. Schowalter, and P. M. Ajayan, “Vertically aligned conductive carbon nanotube junctions and arrays for device applications,” *Appl. Phys. Lett.*, vol. 84, no. 15, pp. 2889–2891, Apr. 2004.
- [54] L. B. Kish and P. M. Ajayan, “TerraByte flash memory with carbon nanotubes,” *Appl. Phys. Lett.*, vol. 86, no. 9, pp. 093106–093106–2, Feb. 2005.
- [55] S. Pramanik, S. Bandyopadhyay, K. Garre, and M. Cahay, “Normal and inverse spin-valve effect in organic semiconductor nanowires and the background monotonic magnetoresistance,” *Phys. Rev. B*, vol. 74, no. 23, p. 235329, Dec. 2006.
- [56] K. M. Alam, S. C. Bodepudi, R. Starko-Bowes, and S. Pramanik, “Suppression of spin relaxation in rubrene nanowire spin valves,” *Appl. Phys. Lett.*, vol. 101, no. 19, pp. 192403–192403–5, Nov. 2012.
- [57] K. Tsukagoshi, B. W. Alphenaar, and H. Ago, “Coherent transport of electron spin in a ferromagnetically contacted carbon nanotube,” *Nature*, vol. 401, no. 6753, pp. 572–574, Oct. 1999.
- [58] L. E. Hueso, J. M. Pruneda, V. Ferrari, G. Burnell, J. P. Valdés-Herrera, B. D. Simons, P. B. Littlewood, E. Artacho, A. Fert, and N. D. Mathur, “Transformation of spin information into large electrical signals using carbon nanotubes,” *Nature*, vol. 445, no. 7126, pp. 410–413, Jan. 2007.
- [59] R. Thamankar, S. Niyogi, B. Y. Yoo, Y. W. Rheem, N. V. Myung, R. C. Haddon, and R. K. Kawakami, “Spin-polarized transport in magnetically assembled carbon nanotube spin valves,” *Appl. Phys. Lett.*, vol. 89, no. 3, pp. 033119–033119–3, Jul. 2006.
- [60] H. Aurich, A. Baumgartner, F. Freitag, A. Eichler, J. Trbovic, and C. Schönenberger, “Permalloy-based carbon nanotube spin-valve,” *Appl. Phys. Lett.*, vol. 97, no. 15, pp. 153116–153116–3, Oct. 2010.
- [61] J. D. Bergeson, S. J. Etzkorn, M. B. Murphey, L. Qu, J. Yang, L. Dai, and A. J. Epstein, “Iron nanoparticle driven spin-valve behavior in aligned carbon nanotube arrays,” *Appl. Phys. Lett.*, vol. 93, no. 17, pp. 172505–172505–3, Oct. 2008.
- [62] H. Yang, M. E. Itkis, R. Moriya, C. Rettner, J.-S. Jeong, D. S. Pickard, R. C. Haddon, and S. S. P. Parkin, “Nonlocal spin transport in single-walled carbon nanotube networks,” *Phys. Rev. B*, vol. 85, no. 5, p. 052401, Feb. 2012.
- [63] M. Gobbi, F. Golmar, R. Llopis, F. Casanova, and L. E. Hueso, “Room-Temperature Spin Transport in C60-Based Spin Valves,” *Adv. Mater.*, vol. 23, no. 14, pp. 1609–1613, 2011.
- [64] R. Lin, F. Wang, M. Wohlgenannt, C. He, X. Zhai, and Y. Suzuki, “Organic spin-valves based on fullerene C60,” *Synth. Met.*, vol. 161, no. 7–8, pp. 553–557, Apr. 2011.
- [65] T. L. A. Tran, T. Q. Le, J. G. M. Sanderink, W. G. van der Wiel, and M. P. de Jong, “The Multistep Tunneling Analogue of Conductivity Mismatch in Organic Spin Valves,” *Adv. Funct. Mater.*, vol. 22, no. 6, pp. 1180–1189, 2012.
- [66] Z. G. Yu, “Spin-orbit coupling and its effects in organic solids,” *Phys. Rev. B*, vol. 85, no. 11, p. 115201, Mar. 2012.

- [67] R. Starko-Bowes, S. C. Bodepudi, K. M. Alam, A. P. Singh, and S. Pramanik, "Room temperature spin valve effect in highly ordered array of methanofullerene nanotubes," *J. Appl. Phys.*, vol. 114, no. 4, pp. 044316–044316–9, Jul. 2013.
- [68] R. O. Al-Kaysi, T. H. Ghaddar, and G. Guirado, "Fabrication of One-Dimensional Organic Nanostructures Using Anodic Aluminum Oxide Templates," *J. Nanomater.*, vol. 2009, Apr. 2009.
- [69] Z. V. Vardeny, Ed., *Organic Spintronics*, 1st ed. CRC Press, 2010.
- [70] I. Bergenti, V. Dediu, M. Prezioso, and A. Riminucci, "Organic Spintronics," *Philos. Trans. R. Soc. Math. Phys. Eng. Sci.*, vol. 369, no. 1948, pp. 3054–3068, Aug. 2011.
- [71] C. R. Martin, "Nanomaterials: a membrane-based synthetic approach.," *Science*, Dec. 1994.
- [72] S. Pramanik, B. Kanchibotla, S. Sarkar, G. Tepper, and S. Bandyopadhyay, "Electrochemical Self-Assembly of Nanostructures: Fabrication and Device Applications," in *Encyclopedia of Nanoscience and Nanotechnology*, vol. 13, 2011, pp. 273–32.
- [73] Kanchibotla, B., Pramanik, S., Bandyopadhyay, S., "Self-assembly of nanostructures using nanoporous alumina template," in *Nano and molecular electronics handbook (Chapter 9)*, 2007.
- [74] D. Zhang, L. Luo, Q. Liao, H. Wang, H. Fu, and J. Yao, "Polypyrrole/ZnS Core/Shell Coaxial Nanowires Prepared by Anodic Aluminum Oxide Template Methods," *J. Phys. Chem. C*, vol. 115, no. 5, pp. 2360–2365, Feb. 2011.
- [75] S. Valizadeh, J. . George, P. Leisner, and L. Hultman, "Electrochemical deposition of Co nanowire arrays; quantitative consideration of concentration profiles," *Electrochimica Acta*, vol. 47, no. 6, pp. 865–874, Dec. 2001.
- [76] J. W. Diggle, T. C. Downie, and C. W. Goulding, "Anodic oxide films on aluminum," *Chem. Rev.*, vol. 69, no. 3, pp. 365–405, Jun. 1969.
- [77] M. Steinhart, R. B. Wehrspohn, U. Gösele, and J. H. Wendorff, "Nanotubes by Template Wetting: A Modular Assembly System," *Angew. Chem. Int. Ed.*, vol. 43, no. 11, pp. 1334–1344, 2004.
- [78] J. W. Lee, K. Kim, D. H. Park, M. Y. Cho, Y. B. Lee, J. S. Jung, D. Kim, J. Kim, and J. Joo, "Light-Emitting Rubrene Nanowire Arrays: A Comparison with Rubrene Single Crystals," *Adv. Funct. Mater.*, vol. 19, no. 5, pp. 704–710, Mar. 2009.
- [79] H. Liu, Y. Li, L. Jiang, H. Luo, S. Xiao, H. Fang, H. Li, D. Zhu, D. Yu, J. Xu, and B. Xiang, "Imaging As-Grown [60]Fullerene Nanotubes by Template Technique," *J. Am. Chem. Soc.*, vol. 124, no. 45, pp. 13370–13371, Nov. 2002.
- [80] J. C. Hulthen and C. R. Martin, "A general template-based method for the preparation of nanomaterials," *J. Mater. Chem.*, vol. 7, no. 7, pp. 1075–1087, Jan. 1997.
- [81] K. M. Alam, A. P. Singh, S. C. Bodepudi, and S. Pramanik, "Fabrication of hexagonally ordered nanopores in anodic alumina: An alternative pretreatment," *Surf. Sci.*, vol. 605, no. 3–4, pp. 441–449, Feb. 2011.
- [82] H. Masuda, F. Hasegawa, and S. Ono, "Self-Ordering of Cell Arrangement of Anodic Porous Alumina Formed in Sulfuric Acid Solution," *J. Electrochem. Soc.*, vol. 144, no. 5, pp. L127–L130, May 1997.
- [83] H. M. Stec, R. J. Williams, T. S. Jones, and R. A. Hatton, "Ultrathin Transparent Au Electrodes for Organic Photovoltaics Fabricated Using a Mixed Mono-Molecular Nucleation Layer," *Adv. Funct. Mater.*, vol. 21, no. 9, pp. 1709–1716, 2011.

- [84] H. J. Oh, Y. S. Jeong, S. H. Kwon, C. H. Heo, B. S. Ki, and C. S. Chi, "Fabrication of Polymer Nanotubes Using Alumina Template," *Solid State Phenom.*, vol. 124–126, pp. 1109–1112, 2007.
- [85] S. C. Bodepudi, D. Bachman, and S. Pramanik, "Fabrication of Highly Ordered Cylindrical Nanopores with Modulated Diameter Using Anodic Alumina," in *2011 International Conference on Nanoscience, Technology and Societal Implications (NSTSI)*, 2011, pp. 1–4.
- [86] A. Vlad, S. Melinte, M. Mátéfi-Tempfli, L. Piraux, and S. Mátéfi-Tempfli, "Vertical Nanowire Architectures: Statistical Processing of Porous Templates Towards Discrete Nanochannel Integration," *Small*, vol. 6, no. 18, pp. 1974–1980, 2010.
- [87] S. H. Jo, K.-H. Kim, and W. Lu, "High-Density Crossbar Arrays Based on a Si Memristive System," *Nano Lett.*, vol. 9, no. 2, pp. 870–874, Feb. 2009.
- [88] J. H. Lee, D. W. Kim, H. Jang, J. K. Choi, J. Geng, J. W. Jung, S. C. Yoon, and H.-T. Jung, "Enhanced solar-cell efficiency in bulk-heterojunction polymer systems obtained by nanoimprinting with commercially available AAO membrane filters," *Small Weinh. Bergstr. Ger.*, vol. 5, no. 19, pp. 2139–2143, Oct. 2009.
- [89] J. E. Allen and C. T. Black, "Improved Power Conversion Efficiency in Bulk Heterojunction Organic Solar Cells with Radial Electron Contacts," *ACS Nano*, vol. 5, no. 10, pp. 7986–7991, 2011.
- [90] D. M. O'Carroll, J. S. Fakonas, D. M. Callahan, M. Schierhorn, and H. A. Atwater, "Metal-Polymer-Metal Split-Dipole Nanoantennas," *Adv. Mater.*, vol. 24, no. 23, pp. OP136–OP142, 2012.
- [91] J. Y. Zheng, Y. Yan, X. Wang, W. Shi, H. Ma, Y. S. Zhao, and J. Yao, "Hydrogen Peroxide Vapor Sensing with Organic Core/Sheath Nanowire Optical Waveguides," *Adv. Mater.*, vol. 24, no. 35, pp. OP194–OP199, 2012.
- [92] L. Zhang, F. Meng, Y. Chen, J. Liu, Y. Sun, T. Luo, M. Li, and J. Liu, "A novel ammonia sensor based on high density, small diameter polypyrrole nanowire arrays," *Sensors Actuators B Chem.*, vol. 142, no. 1, pp. 204–209, Oct. 2009.
- [93] Q. H. Cui, L. Jiang, C. Zhang, Y. S. Zhao, W. Hu, and J. Yao, "Coaxial Organic p-n Heterojunction Nanowire Arrays: One-Step Synthesis and Photoelectric Properties," *Adv. Mater.*, vol. 24, no. 17, pp. 2332–2336, 2012.
- [94] B. Kippelen and J.-L. Brédas, "Organic photovoltaics," *Energy Environ. Sci.*, vol. 2, no. 3, pp. 251–261, Mar. 2009.
- [95] K. M. Coakley and M. D. McGehee, "Conjugated Polymer Photovoltaic Cells," *Chem Mater*, vol. 16, no. 23, pp. 4533–4542, 2004.
- [96] S. Lach, A. Altenhof, K. Tarafder, F. Schmitt, M. E. Ali, M. Vogel, J. Sauther, P. M. Oppeneer, and C. Ziegler, "Metal-Organic Hybrid Interface States of A Ferromagnet/Organic Semiconductor Hybrid Junction as Basis For Engineering Spin Injection in Organic Spintronics," *Adv. Funct. Mater.*, vol. 22, no. 5, pp. 989–997, Mar. 2012.
- [97] Y. Zhan, E. Holmström, R. Lizárraga, O. Eriksson, X. Liu, F. Li, E. Carlegrim, S. Stafström, and M. Fahlman, "Efficient Spin Injection Through Exchange Coupling at Organic Semiconductor/Ferromagnet Heterojunctions," *Adv. Mater.*, vol. 22, no. 14, pp. 1626–1630, Apr. 2010.
- [98] J. Brede, N. Atodiresei, S. Kuck, P. Lazić, V. Caciuc, Y. Morikawa, G. Hoffmann, S. Blügel, and R. Wiesendanger, "Spin- and Energy-Dependent Tunneling through a Single Molecule with Intramolecular Spatial Resolution," *Phys. Rev. Lett.*, vol. 105, no. 4, p. 047204, Jul. 2010.
- [99] M. Cinchetti, S. Neuschwander, A. Fischer, A. Ruffing, S. Mathias, J.-P. Wüstenberg, and M. Aeschlimann, "Tailoring the Spin Functionality of a Hybrid

- Metal–Organic Interface by Means of Alkali–Metal Doping,” *Phys. Rev. Lett.*, vol. 104, no. 21, p. 217602, May 2010.
- [100] C. Barraud, P. Seneor, R. Mattana, S. Fusil, K. Bouzehouane, C. Deranlot, P. Graziosi, L. Hueso, I. Bergenti, V. Dediu, F. Petroff, and A. Fert, “Unravelling the role of the interface for spin injection into organic semiconductors,” *Nat. Phys.*, vol. 6, no. 8, pp. 615–620, Jun. 2010.
- [101] J.-W. Yoo, H. W. Jang, V. N. Prigodin, C. Kao, C. B. Eom, and A. J. Epstein, “Giant magnetoresistance in ferromagnet/organic semiconductor/ferromagnet heterojunctions,” *Phys. Rev. B*, vol. 80, no. 20, p. 205207, Nov. 2009.
- [102] R. Lin, F. Wang, J. Rybicki, M. Wohlgenannt, and K. A. Hutchinson, “Distinguishing between tunneling and injection regimes of ferromagnet/organic semiconductor/ferromagnet junctions,” *Phys. Rev. B*, vol. 81, no. 19, p. 195214, May 2010.
- [103] J. H. Shim, K. V. Raman, Y. J. Park, T. S. Santos, G. X. Miao, B. Satpati, and J. S. Moodera, “Large Spin Diffusion Length in an Amorphous Organic Semiconductor,” *Phys. Rev. Lett.*, vol. 100, no. 22, p. 226603, Jun. 2008.
- [104] Z. H. Xiong, D. Wu, Z. Vally Vardeny, and J. Shi, “Giant magnetoresistance in organic spin-valves,” *Nature*, vol. 427, no. 6977, pp. 821–824, Feb. 2004.
- [105] V. Dediu, L. E. Hueso, I. Bergenti, A. Riminucci, F. Borgatti, P. Graziosi, C. Newby, F. Casoli, M. P. De Jong, C. Taliani, and Y. Zhan, “Room-temperature spintronic effects in Alq₃-based hybrid devices,” *Phys. Rev. B*, vol. 78, no. 11, p. 115203, Sep. 2008.
- [106] Y. Liu, S. M. Watson, T. Lee, J. M. Gorham, H. E. Katz, J. A. Borchers, H. D. Fairbrother, and D. H. Reich, “Correlation between microstructure and magnetotransport in organic semiconductor spin-valve structures,” *Phys. Rev. B*, vol. 79, no. 7, p. 075312, Feb. 2009.
- [107] Y. Zhang, T. P. Basel, B. R. Gautam, X. Yang, D. J. Mascaró, F. Liu, and Z. V. Vardeny, “Spin-enhanced organic bulk heterojunction photovoltaic solar cells,” *Nat. Commun.*, vol. 3, p. 1043, Sep. 2012.
- [108] B. T. Jonker, G. Kioseoglou, A. T. Hanbicki, C. H. Li, and P. E. Thompson, “Electrical spin-injection into silicon from a ferromagnetic metal/tunnel barrier contact,” *Nat. Phys.*, vol. 3, no. 8, pp. 542–546, Aug. 2007.
- [109] M. P. Vincenzo Schettino, “The Vibrational Spectrum of fullerene C₆₀,” *J Phys Chem*, vol. 105, pp. 11192–11196, 2001.
- [110] Y. Lee, S. H. Lee, K. Kim, J. W. Lee, K.-Y. Han, J. Kim, and J. Joo, “Single nanoparticle of organic p-type and n-type hybrid materials: nanoscale phase separation and photovoltaic effect,” *J. Mater. Chem.*, vol. 22, no. 6, pp. 2485–2490, Jan. 2012.
- [111] M. Chikamatsu, S. Nagamatsu, Y. Yoshida, K. Saito, K. Yase, and K. Kikuchi, “Solution-processed n-type organic thin-film transistors with high field-effect mobility,” *Appl. Phys. Lett.*, vol. 87, no. 20, p. 203504, 2005.
- [112] B. Xue, B. Vaughan, C.-H. Poh, K. B. Burke, L. Thomsen, A. Stapleton, X. Zhou, G. W. Bryant, W. Belcher, and P. C. Dastoor, “Vertical Stratification and Interfacial Structure in P3HT:PCBM Organic Solar Cells,” *J. Phys. Chem. C*, vol. 114, no. 37, pp. 15797–15805, Sep. 2010.
- [113] F. Burke, P. Stamenov, and J. M. D. Coey, “Charge injection, transport and localization in rubrene,” *Synth. Met.*, vol. 161, no. 7–8, pp. 563–569, Apr. 2011.
- [114] J. C. Scott, “Metal–organic interface and charge injection in organic electronic devices,” *J. Vac. Sci. Technol. Vac. Surfaces Films*, vol. 21, no. 3, pp. 521–531, 2003.

- [115] A. Molinari, I. Gutiérrez, I. N. Hulea, S. Russo, and A. F. Morpurgo, “Bias-dependent contact resistance in rubrene single-crystal field-effect transistors,” *Appl. Phys. Lett.*, vol. 90, no. 21, pp. 212103–212103–3, May 2007.
- [116] M. Tzolov, B. Chang, A. Yin, D. Straus, J. M. Xu, and G. Brown, “Electronic Transport in a Controllably Grown Carbon Nanotube-Silicon Heterojunction Array,” *Phys. Rev. Lett.*, vol. 92, no. 7, p. 075505, Feb. 2004.
- [117] T. D. Nguyen, Y. Sheng, M. Wohlgenannt, and T. D. Anthopoulos, “On the role of hydrogen in organic magnetoresistance: A study of C60 devices,” *Synth. Met.*, vol. 157, no. 22–23, pp. 930–934, Nov. 2007.
- [118] T. D. Nguyen, F. Wang, X.-G. Li, E. Ehrenfreund, and Z. V. Vardeny, “Spin diffusion in fullerene-based devices: Morphology effect,” *Phys. Rev. B*, vol. 87, no. 7, p. 075205, Feb. 2013.
- [119] S. Lach, A. Altenhof, K. Tarafder, F. Schmitt, M. E. Ali, M. Vogel, J. Sauther, P. M. Oppeneer, and C. Ziegler, “Metal–Organic Hybrid Interface States of A Ferromagnet/Organic Semiconductor Hybrid Junction as Basis For Engineering Spin Injection in Organic Spintronics,” *Adv. Funct. Mater.*, vol. 22, no. 5, pp. 989–997, 2012.
- [120] C. Barraud, P. Seneor, R. Mattana, S. Fusil, K. Bouzehouane, C. Deranlot, P. Graziosi, L. Hueso, I. Bergenti, V. Dediu, F. Petroff, and A. Fert, “Unravelling the role of the interface for spin injection into organic semiconductors,” *Nat. Phys.*, vol. 6, no. 8, pp. 615–620, Aug. 2010.
- [121] T. Ohgai, X. Hoffer, A. Fábíán, L. Gravier, and J.-P. Ansermet, “Electrochemical synthesis and magnetoresistance properties of Ni, Co and Co/Cu nanowires in a nanoporous anodic oxide layer on metallic aluminium,” *J. Mater. Chem.*, vol. 13, no. 10, pp. 2530–2534, Sep. 2003.
- [122] F. G. Monzon and M. L. Roukes, “Spin injection and the local Hall effect in InAs quantum wells,” *J. Magn. Magn. Mater.*, vol. 198–199, pp. 632–635, Jun. 1999.
- [123] Y. Q. Zhan, X. J. Liu, E. Carlegrim, F. H. Li, I. Bergenti, P. Graziosi, V. Dediu, and M. Fahlman, “The role of aluminum oxide buffer layer in organic spin-valves performance,” *Appl. Phys. Lett.*, vol. 94, no. 5, pp. 053301–053301–3, Feb. 2009.
- [124] R. Lin, F. Wang, J. Rybicki, M. Wohlgenannt, and K. A. Hutchinson, “Distinguishing between tunneling and injection regimes of ferromagnet/organic semiconductor/ferromagnet junctions,” *Phys. Rev. B*, vol. 81, no. 19, p. 195214, May 2010.
- [125] E. Y. Tsymbal, O. N. Mryasov, and P. R. LeClair, “Spin-dependent tunnelling in magnetic tunnel junctions,” *J. Phys. Condens. Matter*, vol. 15, no. 4, p. R109, Feb. 2003.
- [126] C. Chappert, A. Fert, and F. N. Van Dau, “The emergence of spin electronics in data storage,” *Nat. Mater.*, vol. 6, no. 11, pp. 813–823, Nov. 2007.
- [127] G. Xiong, J. W. Elam, H. Feng, C. Y. Han, H.-H. Wang, L. E. Iton, L. A. Curtiss, M. J. Pellin, M. Kung, H. Kung, and P. C. Stair, “Effect of atomic layer deposition coatings on the surface structure of anodic aluminum oxide membranes,” *J. Phys. Chem. B*, vol. 109, no. 29, pp. 14059–14063, Jul. 2005.
- [128] G. Yu, J. Gao, J. C. Hummelen, F. Wudl, and A. J. Heeger, “Polymer Photovoltaic Cells: Enhanced Efficiencies via a Network of Internal Donor-Acceptor Heterojunctions,” *Science*, vol. 270, no. 5243, pp. 1789–1791, Dec. 1995.
- [129] C. W. Tang, “Two-layer organic photovoltaic cell,” *Appl. Phys. Lett.*, vol. 48, no. 2, pp. 183–185, Jan. 1986.

Biography

Ryan Starko-Bowes

Education:

M.Sc. in Electrical Engineering (Solid State Electronics)
University of Alberta (2010-2013)

B.Sc. in Engineering Physics (Nanoengineering Option)
University of Alberta (2006-2010)

Publications – Journal Articles (as in Bibliography):

[1], [48], [56], [67]

Publications – Conference Abstracts:

- **Ryan Starko-Bowes**, Sandipan Pramanik, “Methanofullerene Nanotubes for Room Temperature Organic Spintronics”, *Faculty of Engineering Graduate Research Symposium*, University of Alberta, Edmonton, Canada, June 19-20 2013.
- Ward Newman, Srikrishna Bodepudi, Minchang Zhang, **Ryan Starko-Bowes**, Hu Huan, Jonathan Atkinson, Ilya Utkin, Robert Fedosejevs, Ray DeCorby, Sandipan Pramanik, Zubin Jacob, “Characterization of the optical topological transition in 1D (multilayer) and 2D (nanowire) hyperbolic metamaterials”, *SPIE Optics + Photonics 2013*, San Diego Convention Center, San Diego, California, United States, August 25-29 2013.
- **Ryan Starko-Bowes**, Sandipan Pramanik, “Spin Transport Properties of PCBM nanotube spin valves”, *Faculty of Engineering Graduate Research Symposium*, University of Alberta, Edmonton, Canada, June 20-21, 2012.
- **Ryan Starko-Bowes**, Sandipan Pramanik, “Spin Transport Properties of Methanofullerene Nanotube Spin Valves”, *Alberta Graduate Conference*, University of Alberta, Edmonton, Canada, May, 2012. (Winner of top poster in ICT category)
- **Ryan Starko-Bowes**, Sandipan Pramanik, “Vertical array of fullerene nanotube (FNT) spin valves for ultra-high density spintronic memory”, *International Conference on the Science and Application of Nanotubes*, Cambridge, UK, July, 2011.

Awards

Jason Lang Scholarship (U of A)	2009-2010
Knights of Columbus Scholarship	2009-2010
Queen Elizabeth II Scholarship (two time recipient)	2010-2012
Alberta Graduate Student Scholarship	2010
Faculty of Grad Studies Professional Development Grant (U of A)	2011
Profiling Alberta’s Graduate Students Award (U of A)	2011